SAPIENZA
UNIVERSITÀ DI ROMA

Influence of turbulence on flame propagation during dust explosion

Facoltà di Ingegneria Civile e Industriale
Dipartimento di Ingegneria Chimica Materiali Ambiente
Corso di laurea magistrale in Ingegneria Chimica

Elena Asquini
Matricola 1496500

Relatori
Alessandra Adrover
Frederic Heymes

Correlatore
Clement Chanut

A.A. 2018-2019

Contents

List of Figures

List of Tables

Introduction

Dust explosions represent a major risk in all industries dealing with combustible dust. When these powders have sufficiently fine dimensions, they can easily be suspended in the air; in the presence of an ignition source, an explosion may occur. These accidents cost a lot in terms of human lives and financial losses. The measures necessary to avoid it must be implemented.

In order to safeguard the industry from this risk, this phenomenon has to be understood. Safety parameters are important as they allow understanding the level of risk present in an industrial plant and allow designing safety systems that limit the consequences in case of explosion. Models describing flame propagation in the case of gas explosions are now available. With such models, consequences of explosions can be predicted in real accident scenarios. These models can be adapted for the explosions of organic dusts, as these two phenomena exhibit similar combustion mechanisms. Unfortunately the adaptation of the gas flame propagation models is not possible for metal dust; indeed the combustion reaction in this case occurs at the surface of the particles (heterogeneous reaction). Unfortunately, metal dusts give rise to very strong explosion phenomena and are classified as particularly dangerous substances. To construct models suitable for metal dusts experimental data are needed, resulting from studies which aim to a greater understanding of the phenomenon.

This work consists of an experimental study on the influence of dispersion-induced turbulence on aluminum dust flame propagation. To have an explosion of dust, at the moment of ignition, a solid combustible-comburent suspension has to be present. The solid combustible in our case is aluminum powder. The comburent is instead the oxygen of the air.

Dust suspension is an experimental challenge: in order to use the experimental data for

the construction of a numerical model, it is important first to quantify the degree of homogeneity of this suspension; obtaining a homogeneous cloud is preferable. Furthermore, the dust dispersion generates a certain degree of turbulence within the suspension. This turbulence level influences the propagation of the flame, and it is, therefore, necessary to be able to quantify it. The characteristics of the suspension evolve due to the sedimentation of dust, so the phenomenon is non-stationary, and its characterization is complicated.

The experimental study was carried out in the laboratories of the Institute of Risk Sciences of IMT Mines Alès, where a prototype was built specifically to investigate this phenomenon. Within this prototype, a suspension of dust is generated using a special dispersion system.

In the first phase of the work the suspension was characterized: the level of homogeneity in terms of concentration and the level of turbulence were studied. Once the characteristics of the suspension were known, deflagration tests were conducted in the same prototype. The main parameters relating to the explosion were defined and the link between the initial turbulence of the suspension and the characteristics of the explosion was investigated.

In Chapter 1 some fundamental concepts related to the dust explosion phenomenon are recalled. In the first part some generalities on combustible dusts are presented. Subsequently the most important safety parameters in the study of the phenomenon are exposed. A third part focuses on turbulence and its influence on dust explosions. Finally, some experimental studies on the dust explosion are presented focusing on the techniques used to characterize the dust dispersion.

In Chapter 2 the materials and methods that have been used in this work are exposed. The laboratory of Alès made it possible to investigate the characteristics of the

suspension using optical methods since laser and high-speed cameras were available. The suspension was then examined by Mie scattering, to define the homogeneity of the suspension, and by PIV (Particle Image Velocimetry) and LDA (Laser Doppler Anemometry) to determine turbulence levels. The deflagration was investigated using pressure sensors and direct visualization method.

Chapter 3 contains the results of this study. The results of Mie scattering are initially exposed. Subsequently, the results related to the level of turbulence measured in the suspension are presented; after a preliminary analysis to improve the PIV measurements, the results of PIV and LDA are then shown. Then the results of the deflagration tests are exposed; the influence of the initial level of turbulence of the suspension at the moment of ignition on flame propagation being investigated.

Chapter 1

Literature review

In this chapter, a literature review on dust explosions is exposed. First, the phenomenon of dust explosion is described. Then safety parameters (sensitivity and severity) are presented. The third part focuses on the influence of turbulence on dust explosion. Finally, experimental methods used in literature to quantify the concentration homogeneity of the dust cloud and the level of dispersion-induced turbulence are exposed.

1. Dust explosions

A chemical explosion is a violent exothermic reaction, happening in an atmosphere in which combustible and oxidizer are mixed. A dust explosion is a particular type of chemical explosion in which the combustible is a finely divided solid dispersed in the air.

1.1 Combustible dust

Different definitions of dust exist depending on the standard used. For instance, the NFPA standard defines dust as a divided solid with typical size less than 420 μm.

All combustible dust, if fine enough, can cause an explosion. Combustible dust is a solid capable of reacting with an oxidizer (in general the oxygen present in the air). Natural and synthetic organic materials (sugar, grain, plastics, etc.), coal and metals (aluminum, magnesium, iron, etc.) are typical examples of combustible dust. All the materials that are already stable oxides, such as carbonates or silicates, cannot cause an explosion. Because of the variety of powders able to produce an explosion, a wide range of industries has to deal with this hazard.

1.2 Dust explosion phenomenon

The dust explosion event requires five elements to take place (Amyotte 2013), as represented in Figure 1.

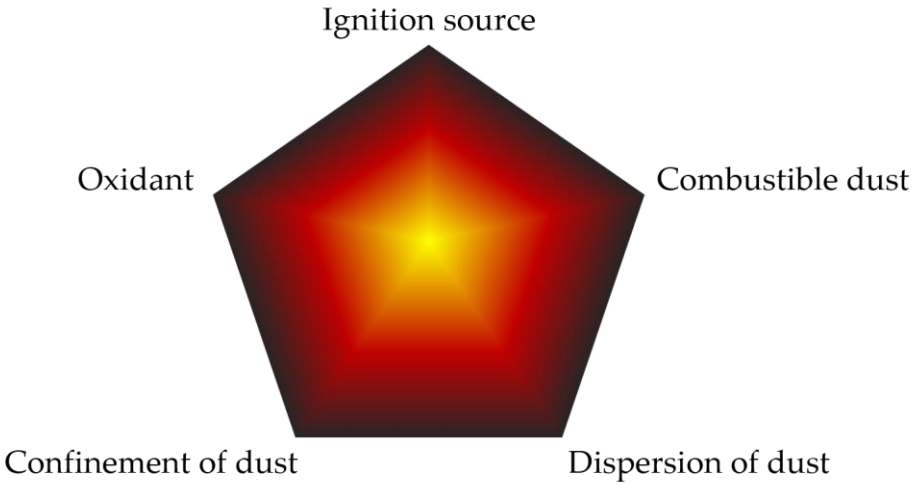

Figure 1: Explosion pentagon

First of all, an oxidant (usually the oxygen from the air), combustible dust and an ignition source have to be present: these three conditions represent the “fire triangle.”

A dust explosion occurs if two more elements are present:

- Dispersion of the dust

An explosion occurs if the dust is suspended in the air. Moreover, for each type of powder, the dust concentration has to be inside a range named "the explosible range". There are several ways in which a dust dispersion can be produced within an industrial process: inside equipment under normal service or due to malfunction; or as a result of a first explosion event. In the latter case, the first explosion disperses the dust settled on the surfaces of the working premises and can generate another destructive blast, called "the secondary explosion".

Dust dispersion is a tricky point in the experimental study of dust explosion because of

its influence on flame propagation.

- Confinement of the dust cloud

This condition is not mandatory, as dust explosions have already been observed without confinement (Julien et al. 2015). However, confinement increases the resulting overpressure and thus the gravity of the explosion.

1.3 Different modes of propagation

Three main modes of propagation can be encountered depending on the combustible dust (Khalili 2018). The first kind of explosion is linked to an oxidation reaction which takes place on the particles surface. This mode of propagation is observed mainly for metallic dust. It results in a heterogeneous reaction between the oxidizer and the solid combustible.

The reaction can also occur in the gaseous phase. In this case, the propagation is divided into two steps. First, dust is pyrolyzed. Then a homogeneous reaction occurs between the combustible (gaseous phase) and the oxygen. This kind of mechanism is observed for sulfur and polyethylene.

The third kind of reaction is a combination of the previous ones. First, a part of the combustible is pyrolyzed ahead of the flame front. This gaseous combustible reacts in homogenous phase with the oxygen. The remaining part of the solid combustible react thanks to the energy released by the combustion. Most of organic dust react following this third mechanism.

1.4 Accidents occurred

As previously mentioned, a wide variety of dust can cause an explosion. Thus, dust explosions can be encountered in several industrial sectors (pharmaceuticals, agri-food, metallurgical, chemicals, etc.).

The dust explosion phenomenon was recognized for the first time in an accident that occurred in 1785 in Turin (Italy), inside a warehouse of a bakery (Bartknecht 1989). Nowadays, such explosions still occur: estimates say that one dust explosion occurs every day in each industrialized country (Proust 2006).
Some accidents occurred in history are presented:

Imperial Sugar Company (USA, 7th February 2008): two explosions occurred in a sugar refinery. A fireball rose above the refinery resulting in a huge fire lasting for 7 days. 14 persons died, and 39 were seriously injured. The first explosion dispersed sugar dust causing a second violent explosion (Vorderbrueggen 2011).

Zhong Rong Metal Products Co (China, 2th August 2014): aluminium-alloy dust explosion, starting from a dust filter and propagating with secondary explosions in the premises of the factory. 146 people killed, 114 injured (Li et al. 2016).

2. Safety Parameters

Potential effects of dust explosions are overpressure, thermal effects, and projectiles. The industrial risk aims to avoid these explosions and to limit the effects in case of an accident. Safety parameters relating to the dust explosion are defined, which represent the starting point for quantifying the probability that the explosion occurs and the extent of damage associated with the potential explosion.

The parameters that quantify the dust sensitivity are useful in the implementation phase of prevention measures within the industry to avoid the occurrence of such an explosion. The main parameters are minimum explosible concentration (MEC), minimum ignition energy (MIE), minimum ignition temperature (MIT).

The parameters that quantify the severity of the explosion represent helpful information to choose the proper protective measures in order to minimize the damage of the potential explosion. The protection parameters are: maximum explosion pressure (Pmax), maximum rate of pressure rise (dP/dtmax), deflagration index (Kst).

These safety parameters (sensitivity and severity) are determined thanks to standardized tests presented hereafter.

2.1 Dust sensitivity

The Minimum Ignition energy (MIE) corresponds to the minimum amount of energy that causes a powder-air suspension to ignite. The ASTM E2019-03 method is commonly used to determine MIE, with a Hartmann tube represented in Figure 2. The test procedure is as follows: the powder, moved by a jet of pressurized air, enters from the base of the prototype through a mushroom disperser. The suspension of dust and air is ignited by an electric arc formed between two electrodes, whose energy can be modified in a specific interval. At the top of the prototype, a cover is positioned allowing the evacuation of the overpressure.

By testing different values of ignition energies and different time at which ignition takes place, the MIE value is determined.

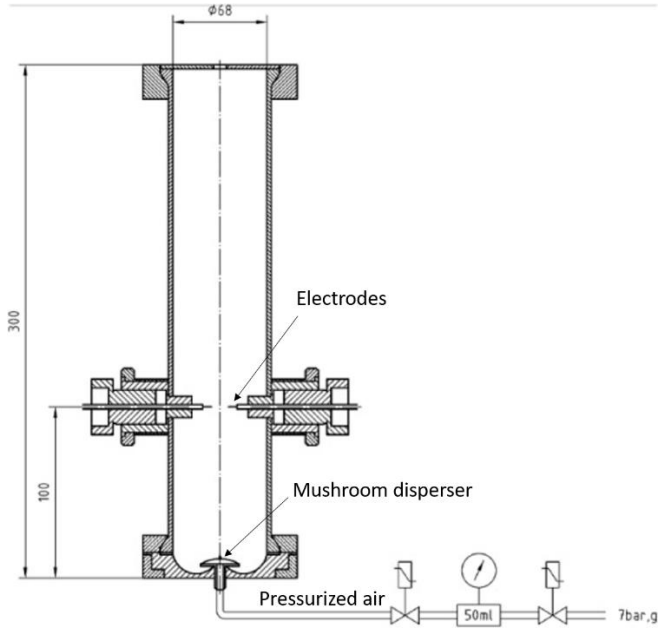

Figure 2: Horizontal cross section of a Hartmann tube (Berg et al. 2018)

The Minimum explosible concentration (MEC) (or lower explosibility limit (LEL)) is the minimum mass of dust dispersed in a certain volume of air capable of propagating a deflagration.

Depending on the equipment used to determine this data, values for the same substance can be different (Eckhoff 2003). In addition to the Hartmann tube previously presented, the 20-L sphere can be used, according to the ASTM E1515-07 method, to obtain a relative measure of MEC. The apparatus scheme is shown in Figure 3.

The test is carried out in the following way: the powder is dispersed in the sphere through a disperser placed at the base of it. The produced suspension is at atmospheric pressure. After about sixty milliseconds from the end of the injection, the suspension is ignited. Ignition occurs by an electric discharge between two electrodes or by pyrotechnic igniters.

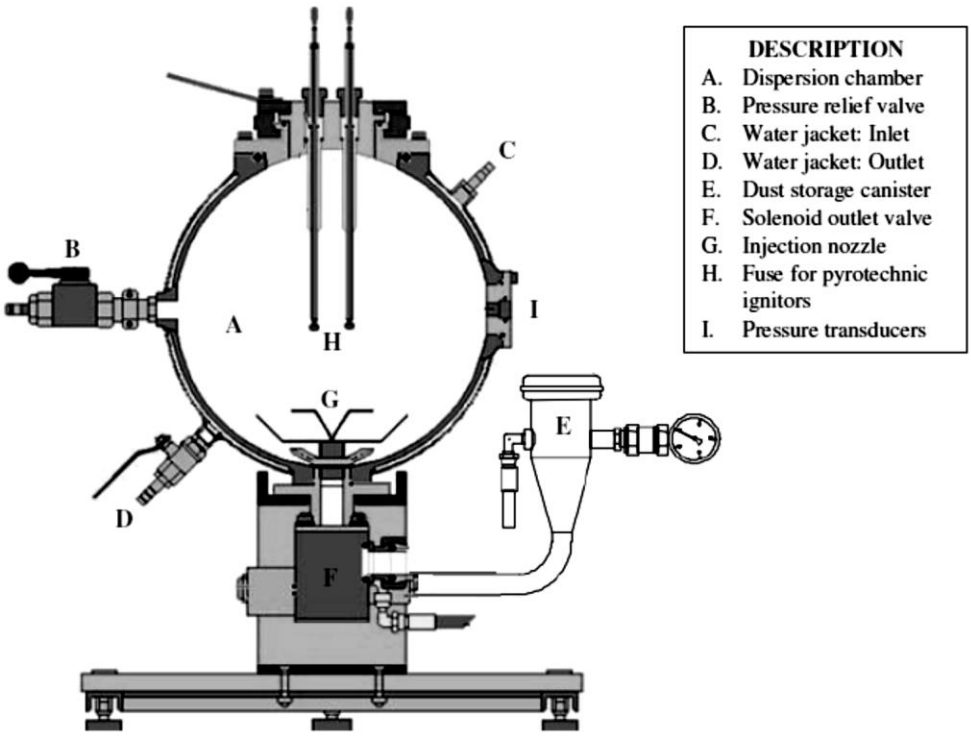

Figure 3: Horizontal cross section of a 20 L Sphere (Murillo 2017)

The Minimum ignition temperature (MIT) is the minimum temperature of a surface which can ignite a dust cloud. This parameter is commonly determined by using the Godbert-Greenwald Furnace (Figure 4). The experimental apparatus consists of a vertical ceramic tube heated by an electrical system, up to a chosen temperature. The MIT is precisely the minimum temperature that triggers the suspension and is determined when a flame is observed.

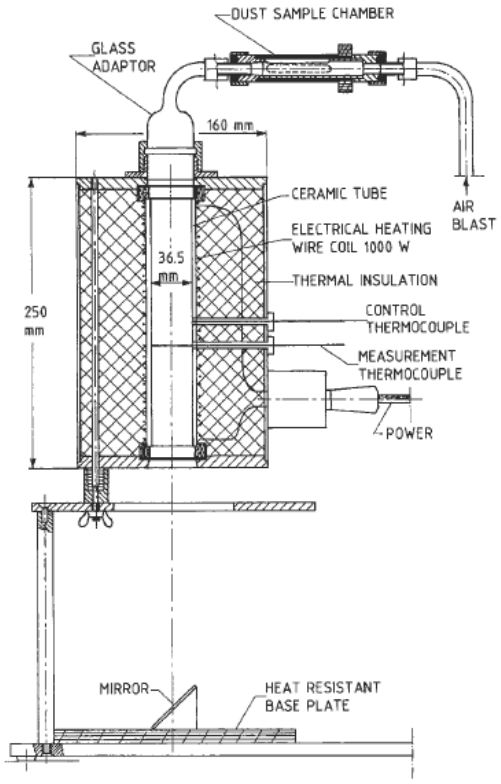

Figure 4: Horizontal cross section of a Godbert-Greenwald Furnace (Eckhoff 2003)

2.2 Explosion severity

Numerous tests have been carried out in standardized closed volume to characterize the explosion behavior of various substances. Through these tests it is possible first to define whether a cloud of dust is capable of propagating a deflagration; furthermore, it is possible to determine the explosibility parameters associated with it.
The 20-liter sphere (ASTM E1226 method) has found widespread use. The typical pressure trend recorded in this type of test is shown in Figure 5.

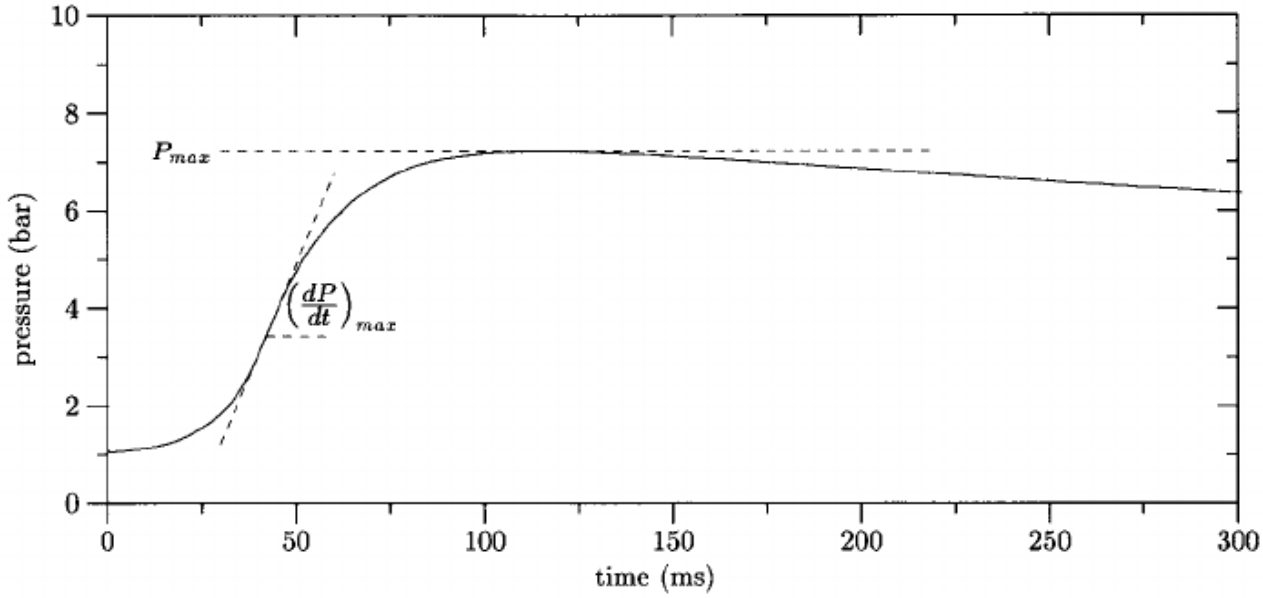

Figure 5: Pressure over time during dust explosion (A. E. Dahoe et al. 2001)

When the dust-air suspension burns inside the closed volume the pressure rises as the flame propagates inside it; when the flame reaches the wall of the confinement, the pressure gets to a maximum value. After this moment the flame exchanges heat with the walls, and there is, therefore, a cooling of the combustion products, and correspondingly a decrease in pressure.

The maximum explosion pressure P_{max}, and the maximum rate of pressure rise $\left(\frac{dP}{dt}\right)_{max}$, permit to have a first estimate of the hazard associated to a particular dust-air suspension.

Both data are used to design the safety devices installed on the equipment, such as the valves and the rupture discs, which allow the evacuation of undesired pressure increases inside the equipment, thus avoiding their catastrophic failure.

The trend of the pressure obtained depends on the geometry of the container used for the measurement. Bartknecht proposed an empirical law, called "cubic law", from the experimental results of combustion of gas mixtures obtained in numerous

configurations. It has been demonstrated experimentally that this law is valid also in the case of mixtures of solid-gas particles (Bozier 2004).

$$K_{st} = \left(\frac{dP}{dt}\right)_{max} . V^{1/3}$$

Kst is called "dust deflagration index" and V is the volume of the vessel used to perform the deflagration. Kst allows the comparison between the explosive violence of different powders (Pu 1988). According to the values of Kst dust can be classified as follow (Kahlili 2018):

Table 1: Dust Hazard classification

Hazard Class	K_{st} (bar m/s)	Characteristic	Typical material
ST 0	<1	No explosion	Silica
ST 1	1-200	Weak explosion	Sugar
ST 2	201-300	Strong explosion	Cellulose
ST 3	>300	Very strong explosion	Aluminium

2.3 Influencing parameters: focus on dust concentration

Safety parameters depend on the features of the dust (nature, size, etc.) and of the environment (temperature, pressure) (Sabard 2013); moreover, they are influenced by the characteristics of the dust-air suspension.

In this part, the influence of dust concentration on some safety parameters is presented. Figure 6 shows the evolution of two safety parameters (explosion rate $\left(\frac{dP}{dt}\right)_{max}$ and MIE) with dust concentration in an explosion range limited by the concentrations C_l, and C_u. Both curves present an extremum corresponding to the concentration C_{worst}. At this value the dust-air mixture has the most critical behavior: in this condition, the explosion

is characterized by high explosion rate and low minimum ignition energy.

The C_{worst} is higher than the stoichiometric concentration C_{stoich} due to the incomplete combustion reaction. For dust concentration lower than this worst-case concentration, combustible is the limiting factor: therefore, the explosion rate increases with dust concentration. For dust concentration higher than C_{stoich}, oxygen is the limiting factor: the explosion rate decreases as concentration increases. An opposite trend is observed for the MIE curve.

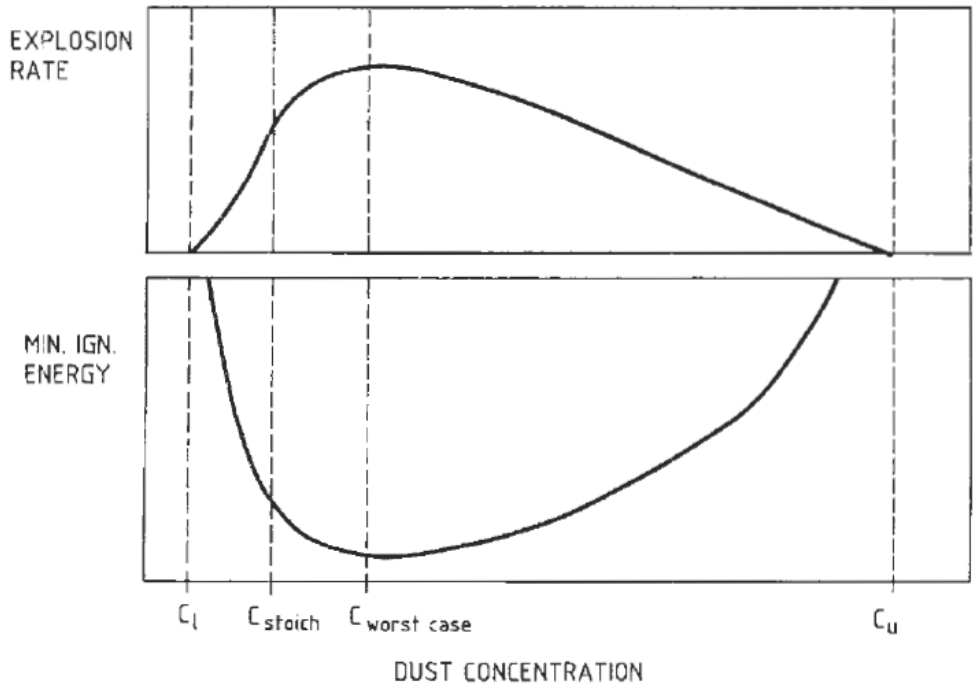

Figure 6: Illustration of evolution of explosion rate MIE with dust concentration (Eckhoff 2003)

3. Influence of turbulence on dust explosion

As previously mentioned, to cause an explosion, the dust has to be dispersed. Experimentally, this dispersion of the dust creates an initial level of turbulence at the moment of ignition. In this part, generalities on turbulence are exposed. Then, some generalities on flames are presented. Finally, the influence of turbulence on severity parameters is detailed.

3.1 Generalities on turbulence

Turbulent flows are characterized by rotating structures, called eddies, which are associated with a length and a time scale. According to the theory formalized by Kolmogorov (Skjold 2003), larger-sized eddies have kinetic energy, which is transferred gradually to smaller rotating structures, through a phenomenon called vortex stretching. The large eddies, more unstable due to the high energy content, break and become smaller and smaller until they disappear by viscous dissipation. Turbulence is, in fact, a dissipative phenomenon, as there is a transfer of kinetic energy from the macroscopic flow to molecular movement.

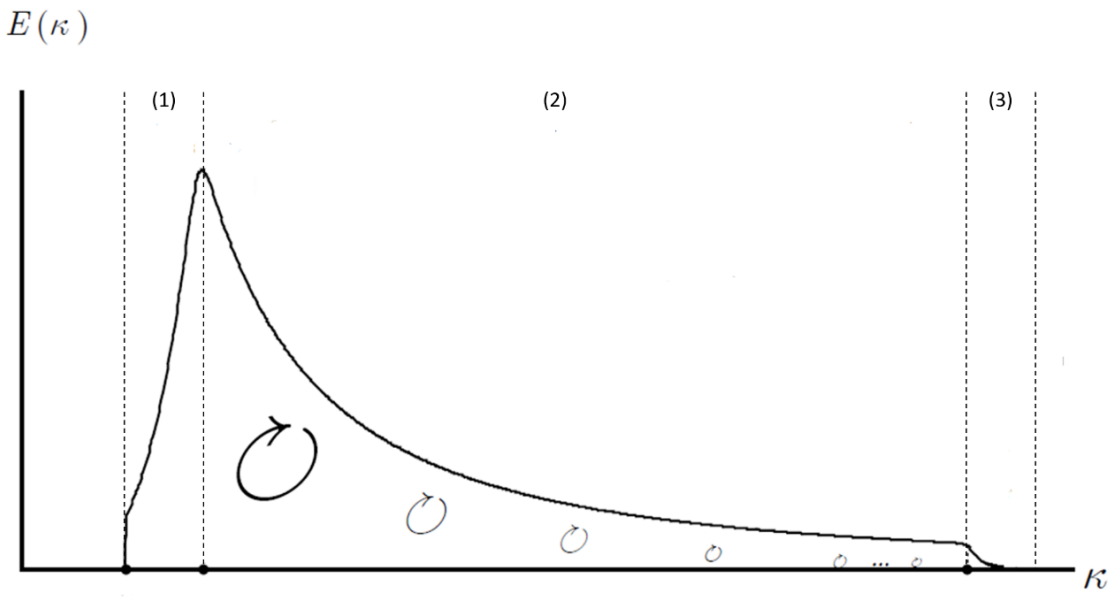

Figure 7: Kolmogorov cascade (elaboration from Skjold 2003)

Figure 7 shows the energy spectrum of the turbulent flow. The wave number k is linked to the size of the eddies; it is, in fact, the reciprocal of their length scale. Low values of k are associated with large eddies. The energy spectrum can be divided into three zones. In the first zone (Figure 7, 1), the energy is produced by the speed gradients present in the flow. Large eddies are present in this zone. In the second one (Figure 7, 2), the energy exchange is associated with breaking large eddies to form smaller eddies; the trend of E(k) on this second zone is:

$$E(k) = k^{-\frac{5}{3}}$$

Finally, on the right, there is a third area (Figure 7,3) where viscous phenomena dissipates energy associated with smaller eddies.

Turbulent flow can be described thanks to Reynolds decomposition. The instantaneous velocity (U) can be separated in a mean component ($\bar{U}$) and a fluctuating component of velocity (u):

$$U(x, y, z, t) = \bar{U}(x, y, z, t) + u(x, y, z, t)$$

From the fluctuating component, the turbulence intensity of the flow (IT) can be calculated:

$$IT(x, y, z, t) = \sqrt{\bar{u}(x, y, z, t)^2}$$

3.2 Generalities on flames

Combustion reactions are classified into two main categories. In premixed combustion, combustible and oxidizer are well mixed before the ignition, a premixed flame appears. A controlled premixed flame is visible from a Bunsen Burner; an uncontrolled premixed flame occurs in the case of explosions. In non-premixed combustion, combustible and oxidizer are divided in the moment of ignition, and the flame is called "diffusion flame" referring to the continuous diffusion of both oxidizer and combustible toward the flame itself (Arief Edsel Dahoe 2000).

Figure 8 exposes the example of a premixed flame propagating in a tube. The flame is the area that divides the gases that have already reacted (burned gases) from those that have yet to react (fresh gases). The flame front will move from the ignition point of the mixture to the area where the gases are still fresh.

Figure 8: Schematic representation of flame propagating in a tube

Figure 9 shows the structure of a laminar flame. The flame front can be divided in two parts: a preheating zone and a reaction zone. In the preheating zone, thanks to the heat conduction and the mass diffusion, the temperature of the fresh gases (T_i) increases up to the ignition temperature of the mixture (T_{ign}). Combustion takes place in the reaction

zone, producing high temperature burned gases.

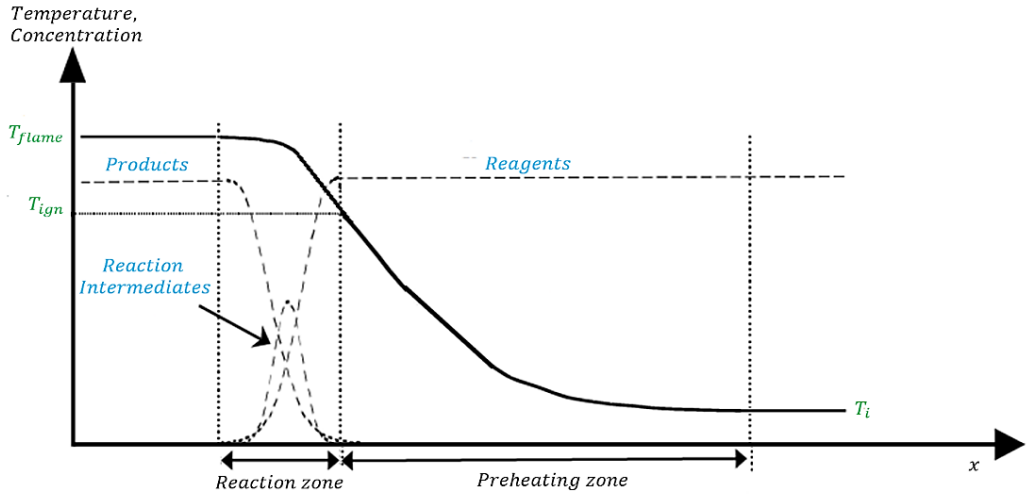

Figure 9: Structure of a laminar flame, elaboration from Sabard 2013

The propagation velocity, V_p, is the velocity of the flame with respect to an external fixed reference. Observing the movement of the flame in the frame of the flow of the fresh gas mixture, a flame arriving at a speed called laminar burning velocity S_{uL} is observed. This burning velocity represents the speed of consumption of the reactants by the flame front and is an intrinsic characteristic of the combustible mixture.

The thickness of the flame δ_L, which includes both the reaction and the preheating zones of the flame, also represents an intrinsic characteristic of the mixture. This thickness can be calculated considering the laminar burning velocity and a chemical time scale τ_c

$$\delta_L = S_{uL} * \tau_c$$

τ_c represents the time interval required to convert the fresh gas mixture into combustion products.

If the flame propagation happens in a combustible mixture characterized by a certain degree of turbulence, the whirling structures of the flow will cause a deformation of the flame. When the combustible mixture is a solid particle-air suspension, dust dispersion always generates a certain degree of turbulence, and the flame propagation will be

affected by this turbulence level.

A turbulent combustion speed S_T is then defined. This speed is not an intrinsic property of the combustible mixture, as it depends also on the characteristics of the flow.

Many relationships have been proposed between the turbulent combustion speed and the laminar burning velocity, as for example the following one:

$$\frac{S_T}{S_{uL}} = 1 + C * \left(\frac{v'_{RMS}}{S_{uL}}\right)^n$$

v'_{RMS} is the root mean square of the turbulence velocity fluctuations, C and n are empirical constants (Arief Edsel Dahoe 2000).

3.3 Influence of dispersion-induced turbulence on severity parameters

To experimentally study a dust explosion, dust has to be dispersed before ignition. This dispersion creates a certain level of turbulence inside the suspension. With time from the end of the suspension generation, the level of turbulence induced by the dispersion system decreases. As shown in Figure 10, related to corn-starch dust behavior, turbulence intensity in the horizontal direction (u') and vertical direction (v') have a decreasing trend:

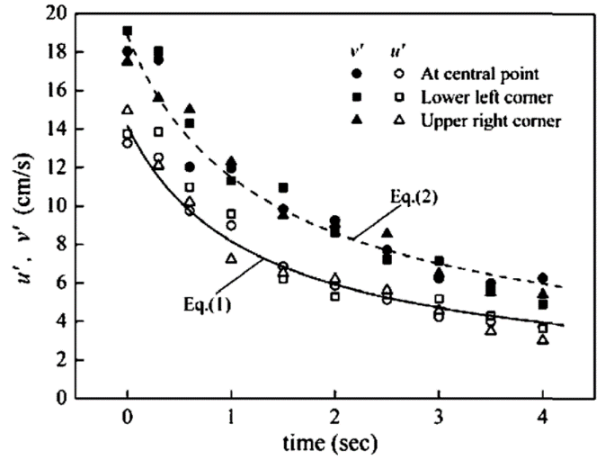

Figure 10: Decay of turbulence level over time (Wang et al. 2006)

Different explosion tests can be carried out modifying the delay between the end of the dispersion of the dust and the ignition of the explosion. This kind of experiments allows the analysis of the link between the severity of the explosion and the initial turbulence level.

Figure 11 shows the evolution of both P_{max} and $\left(\frac{dP}{dt}\right)_{max}$ with the delay between the end of the dust dispersion and the ignition of the dust cloud. As previously mentioned, this delay is linked to the initial level of turbulence: an increase of this delay corresponds to a decrease of initial turbulence. Figure 11 shows that both severity parameters are higher for tests conducted at higher initial turbulence levels. More severe explosion phenomena at higher initial turbulence levels have also been observed by other authors (Tamanini 1990) (Zhang et al. 2016).

The values of severity parameters are higher with turbulent flows because the combustion speed increases with turbulent intensity.

Faster combustion leads to an increase in the rate of pressure rise $\left(\frac{dP}{dt}\right)_{max}$. Moreover, considering the short time available for the flame spread, the deflagration is characterized by a reduction of the thermal losses at the walls of the vessels: this leads to an increase of the maximum overpressure P_{max}.

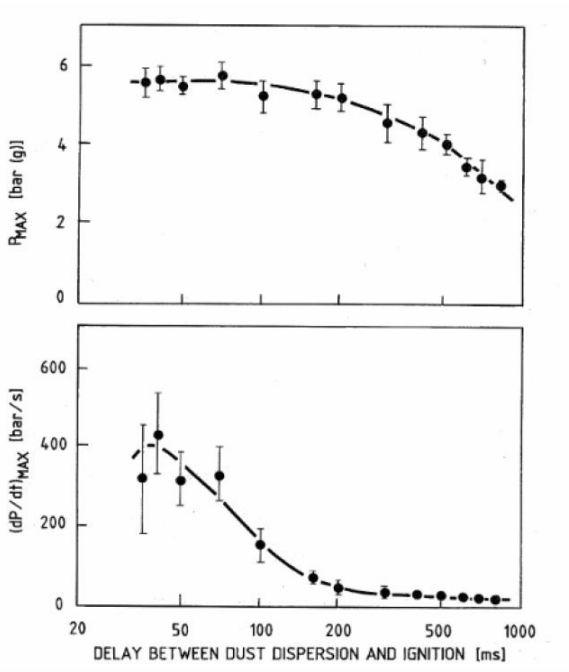

Figure 11: Maximum explosion pressure and maximum rate of pressure rise on delay between dust dispersion and ignition (Eckhoff 2003)

4 Literature review on experimental study of dust dispersion

As previously mentioned, dust dispersion has an important influence on safety parameters. Indeed, both concentration and dispersion-induced turbulence modify these parameters. For this purpose, some authors quantified the concentration homogeneity and the dispersion-induced turbulence inside different prototypes at the moment of ignition. In this part, different methods used to quantify these two quantities are exposed.

4.1 Methods to quantify homogeneity of the suspension before the ignition

The concentration of the dust has a significant influence on the severity of the explosion. Dust concentration is generally calculated by dividing the mass of dust introduced into the vessel, by the volume of the vessel itself. However, it is also important to quantify the homogeneity degree of the dispersion at the moment of ignition.

The optical probes developed by Cashdollar et al. use the principle of light attenuation to measure the concentration of dust clouds (Cashdollar et al.). The essential components of these probes are a light-emitting diode and a photodetector. The probe immersed in the suspension measures the fraction of light transmitted through the cloud, whose value depends on the concentration of dust present. The more the cloud is concentrated, the more the light transmission to the photodetector is hindered.

Kalejaye et al. studied the homogeneity of the dust dispersion generated in the Siwek 20-l chamber (Figure 12) by recording the transmission data obtained with a probe, located at 6 places inside this chamber (Kalejaiye et al. 2010). If the transmission values are similar in the various points of the confinement, the cloud is homogeneous and therefore the dispersion system is efficient.

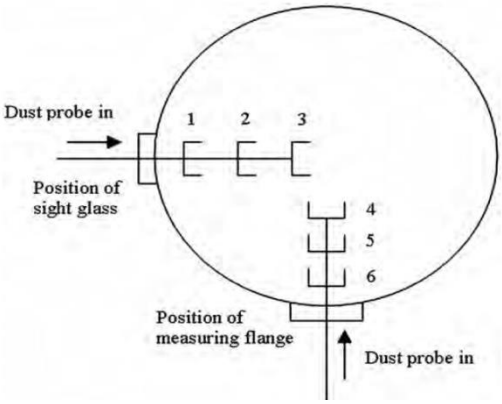

Figure 12: Dust probe locations inside the Siwek 20-L chamber (Kalejaye et al. 2010)

These optical probes also permit to measure the homogeneity of the cloud over time. Their limitation in evaluating the distribution of the dust lies in the fact that they modify the flow as they are inserted inside the vessel. For dispersion chambers that allow the visualization of the phenomenon, the light attenuation can be measured with this kind of probe located outside the vessels. The method used by Vissotski et al. is shown in Figure 13.

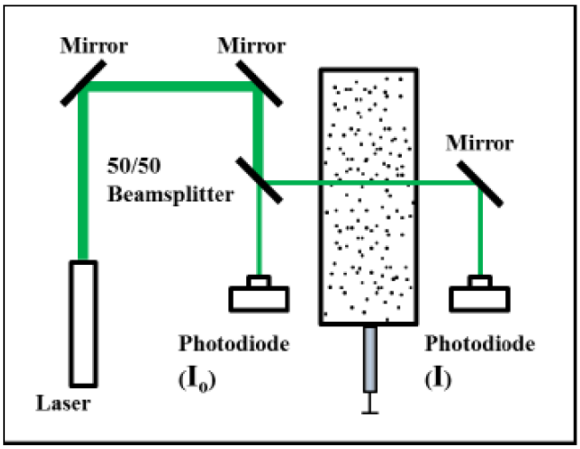

Figure 13: Experimental set up to measure light attenuation (Vissotski et al. 2012)

Two photodiodes measure the intensity of a laser beam before and after crossing the chamber. From the comparison between the recorded values, the amount of light transmitted through the cloud is obtained. From this data, the mean value of dust

concentration is calculated. This method allows obtaining the evolution of concentration over time. Various tests should be performed analyzing different positions to verify homogeneity throughout the chamber.

2D maps of homogeneity levels of dispersion over time can be obtained with Mie scattering technique. The method consists in illuminating the dust cloud with a laser sheet and capturing the light diffused by the particles with a camera (Wu, Liu, and Zhang 2017).

Figure 14: MIE scattering of the suspension at 40,9 ms from the beginning of the dispersion (Bozier 2004)

Figure 14 shows a typical image obtained with Mie scattering technique: the light intensity levels recorded in the images can be related to the concentration of the dust. Areas with a high concentration of dust will give rise to more intense scattering, corresponding to brighter areas in the images.

Mie scattering does not allow only getting the map of homogeneity level of dust in a plane inside the suspension. It also permits to determine its evolution over time. In his thesis, Bozier found a limit of this method regarding the concentration of powder

introduced, which cannot be too high (Bozier 2004).

In the present work, the Mie scattering technique is used to quantify the homogeneity of the dispersion in an experimental apparatus. Therefore this method will be deepened in Chapter 2.

4.2 Methods to quantify turbulence level induced by dispersion

Numerous methods allow obtaining the trend of the decay of the dispersion-induced turbulence inside the suspension. Methods using probes, such as hot wire anemometer or Pitot tubes, allow acquiring the value of the flow velocity in one or more directions: from this value the intensity of the turbulence inside the suspension is calculated. However, the use of these methods has the disadvantage of modifying the flow. The level of turbulence recorded will be then influenced by the measurements.

In the case of an experimental apparatus which permits to visualize the suspension, the measurement of the instantaneous flow velocity can be carried out with optical methods, which do not change the level of turbulence within the flow.

The Particle Image Velocimetry (PIV) and the Laser Doppler Anemometry (LDA) are two optical methods commonly used in dust explosion for the definition of the turbulence level of the suspension.

The Particle Image Velocimetry (PIV) allows building two-dimensional fields of instantaneous velocity in a plane of the flow, with a high spatial resolution. An example of a two-dimensional speed map is shown in Figure 15.

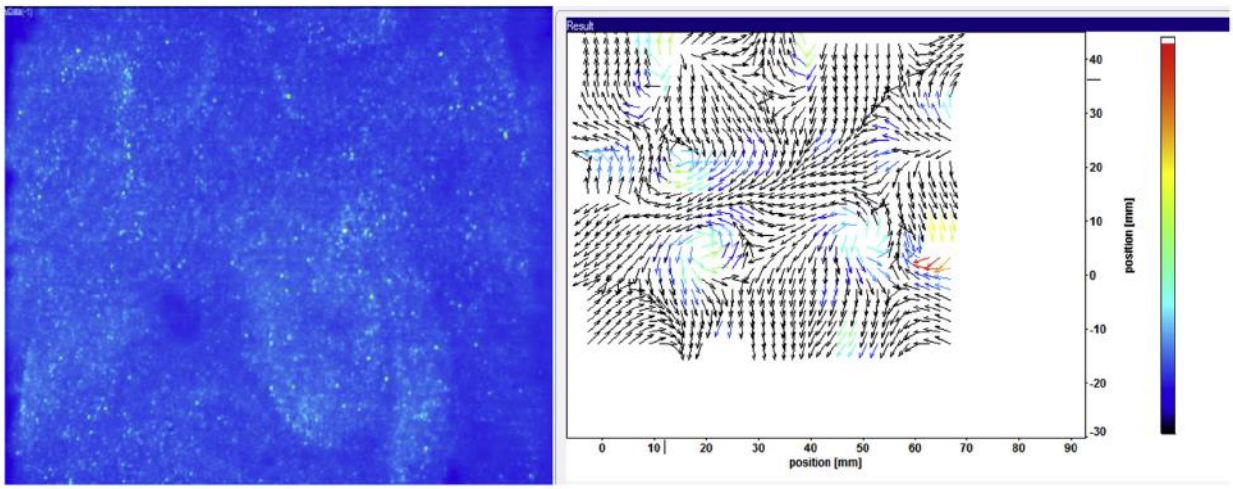

Figure 15: Instantaneous velocity field measured on a plane of the flow (Xu et al. 2017)

The PIV is particularly suitable to study the velocity field of a solid particles-air suspension. In the case of homogeneous liquid or gaseous mixtures, the method requires the addition of tracer particles; in the case of dust suspension, there is no need of adding tracers as they are already inside the flow.

Cuervo (2015) used PIV to characterize the turbulence level of a suspension inside a vertical tube. Cuervo worked with two different chambers. A first one consisted of a transparent casing, 40 cm high, with a section of 7 cm x 7 cm, to view the suspension. The combustion was investigated in the second chamber, higher than the first one to observe the flame propagation (Cuervo 2015). The results of Cuervo were useful for the development of further works, such as that of Murillo, which carried out measurements of PIV inside a 20l sphere (Murillo 2017).

The Laser Doppler Anemometry (LDA) allows obtaining instantaneous velocity values in a localized area of the flow with a high temporal resolution.

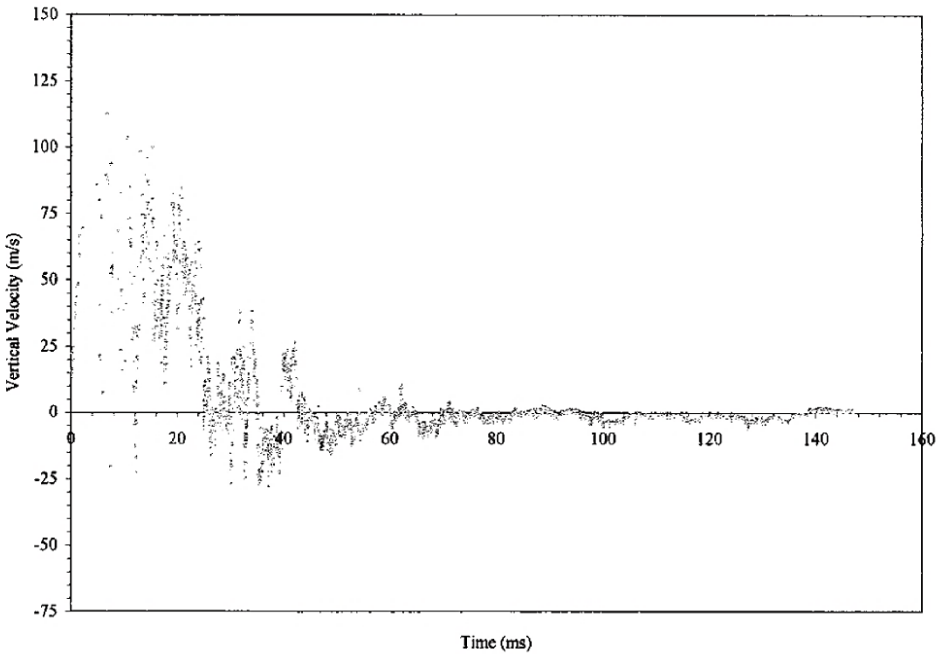

Figure 16: Vertical component of instantaneous velocity in a point of the flow (Mercer et al. 2001)

Figure 16 represents an example of LDV results. As shown in this figure, the data are not homogeneously distributed over time. Indeed, each point is associated with the passage of a solid particle in the area where the measurement is performed. Dahoe et al. (2001) used the LDA to determine the level of turbulence present in the suspension generated inside a 20l explosion sphere. Two velocity components were determined simultaneously. The measurement was performed in six different points of the chamber to verify if the turbulence level within the flow was homogeneous (A. E. Dahoe et al. 2001)

In literature some authors have chosen to investigate the dust dispersion using both the PIV and the LDA, as these two methods are complementary. While the PIV gives a spatial representation of the velocity field, the LDA gives the temporal evolution of the velocity in a point of the flow. The complementary nature of these methods has been highlighted in the work of Galmiche et al. (2013) within a spherical prototype (Galmiche

et al. 2014). Bozier also used both methods to determine the intensity of turbulence inside a vertical tube (Bozier 2004)

The level of turbulence in this work is investigated using both PIV and LDA. Therefore, these methods are presented in details in Chapter 2.

5. Conclusions

Dust explosions represent a significant risk in all industries dealing with combustible powders. All combustible dust, if fine enough and disperse in the air, can cause an explosion. Consequences of such explosions are overpressure, thermal effects, and projectiles.

A first study of the phenomenon consists of evaluating sensitivity and severity parameters. These parameters are obtained with standardized tests. Lots of works allowed obtaining a large quantity of data for a lot of different powders (organic and metallic). These studies are essential for the design of industrial equipment. Indeed, these two parameters allow avoiding the dust explosion (sensibility parameters) or limiting the consequences in case of explosion (severity parameters). Even if these studies cannot allow the modelling of flame propagation during a dust explosion, some influencing factors can be exhibited. Dust concentration and initial turbulence level are two parameters affecting the dust explosion phenomenon.

Models of gaseous flame propagation can be adapted for most of organic dust. However, these models seem not accurate for metallic dust flames. New experiments have to be realized to develop models suitable for metallic dust.

The experimental study of flame propagation in dust explosion requires that the dust has to be dispersed before the ignition. As previously mentioned, this dispersion (concentration and turbulence level) influences the flame propagation. This work aims to study the aluminum dust dispersion (concentration homogeneity and level of turbulence) inside an experimental apparatus specially elaborated to study dust flame propagations. Influence of initial turbulence on aluminum dust flame propagation is also investigated.

Chapter 2
Materials and Methods

1. Materials

1.1 Aluminum dust

Aluminum powder studied in this work is supplied by the company Poudres Hermillon and has a purity of 99.8%. The median diameter of the powder is 6-7 micrometers a granulometric study conducted in the laboratory also confirmed this result (Figure 17).

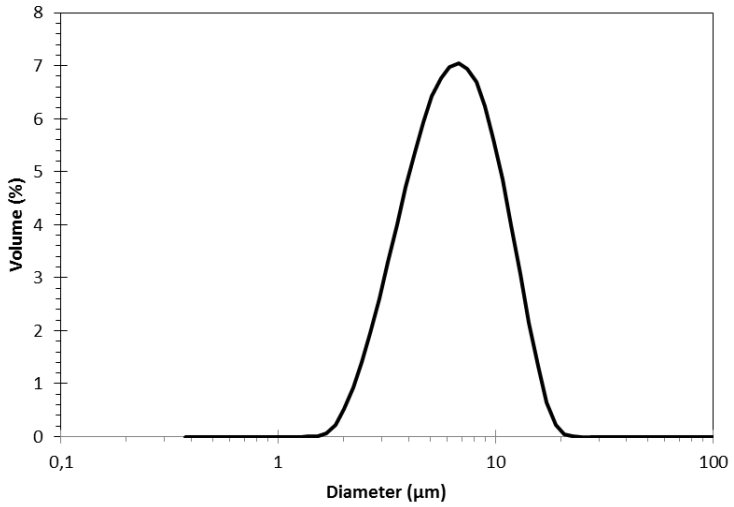

Figure 17: Particle-size distribution of the aluminum powder

Through a Scanning Electron Microscope (SEM) analysis, it is possible to acquire information on the morphology of the particles. Figure 18 shows the images obtained: on the left is represented a 2500x magnification, on the right a 40000x magnification.

The shape of the particles is globally spherical, with a rather smooth surface; the dimensions of the particles are variegated, and some agglomerates are present.

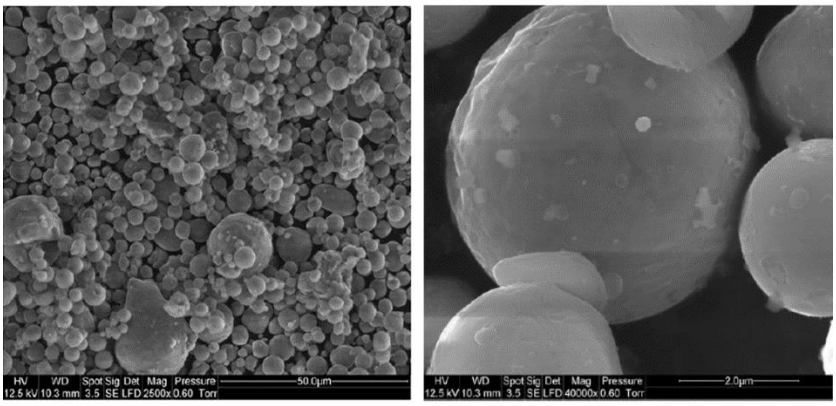

Figure 18: Images of aluminum dust studied, left 2500x, right 40000x

1.2 Experimental Apparatus

An experimental apparatus was built and improved at IMT Mines Alès especially to study aluminum dust dispersion and flame propagation. The prototype and the dispersion system are represented in Figure 19.

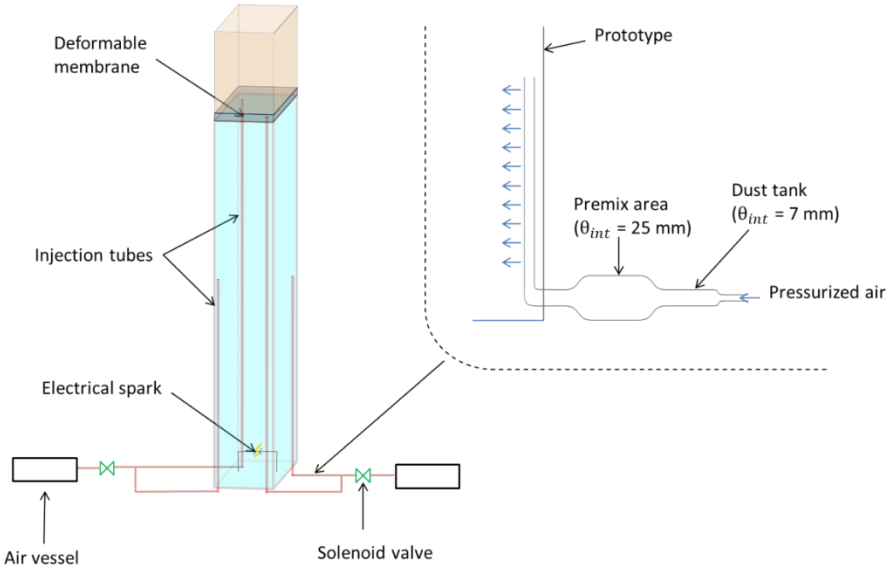

Figure 19: Experimental apparatus scheme

The prototype consists of a chamber with a square section of 15cm x 15 cm and a height of 70 cm. The walls of the chamber are made of glass to visualize the flame and allow

the application of the optical methods to investigate the dust suspension. The thickness of the glass is 10mm to sustain the explosion. The prototype has a metal cage, designed to provide the chamber with mechanical resistance and maximize optical access to each wall. The base of the chamber is 4 cm high and is the area that allows the installation of the dispersion system. Dust dispersion and flame propagation cannot be visualized in this zone.

The dispersion system consists of two compressed air tanks connected to four injection tubes. The tubes are made of copper and have an internal diameter of 7 mm; they are placed at the four corners of the chamber and are characterized by a series of 33 holes through which the suspension enters in the chamber. The holes have a diameter of 2 mm, with a spacing of 1 cm between one hole and the next. The series of holes are oriented towards the center of the prototype. To improve dispersion homogeneity two tubes introduce the powder in the upper part of the prototype, and two in the lower part. The tubes that introduce the powder in the top half of the chamber have holes only on their upper half; those that introduce the dust in the lower part of the chamber have holes in the lower part and are full in their upper part.

The two compressed air tanks have a capacity of 1.1 liters each: the air is discharged into the chamber through the opening of two solenoid valves. Each solenoid valve is connected to two injection tubes.

The powder is placed in four tanks, which are tubes with an internal diameter of 7 mm. These tanks are located between the solenoid valves and the injection tubes. When the air is discharged, it goes through the powder tanks and raises the deposited dust; then it passes through the injection tubes and brings the dust into the chamber. Before entering the injection tubes, the air-powder suspension is premixed; the premixing area consists of tubes with an internal diameter of 25 mm (slowly increasing diameter).

To perform flame propagation, two tungsten electrodes are placed at the base of the prototype. An electric arc between these two electrodes allows the ignition of the dust cloud. The electrodes have a diameter of 2.4 mm and are 4 mm apart. These are located at the height of 13 cm from the base of the prototype.

For ignition, a specific arc generator is used: a high voltage transformer allows ionizing the air present between the two electrodes, thus to create a pre-arc having an energy of the order of 40 mJ and lasting 5 μs. Once the air has been ionized between the electrodes, the discharge of capacitors generates the main arc. This generator allows obtaining an arc with an intensity and a voltage, and therefore a power, almost constant during the entire duration of the arc. The energy of the electric arc can be regulated. It is possible to modify the intensity of the arc (2 A, 4 A or 8 A) but also its duration (from 0.999 ms to 99.9 ms). For each tests, evolutions of intensity and voltage are measured; therefore the energy of the arc is determined for each test. For the tests presented in this manuscript, the intensity is 8A and the duration of the arc is 99.9 ms. The corresponding energy of the arc, measured for each test, is around 13.2 J.

A deformable membrane closes the top of the chamber. This component creates confinement for the suspension so that the calculation of dust concentration at the moment of ignition is made possible. It also permits to keep the atmospheric pressure inside the prototype when the powder-air suspension is injected in the chamber, by increasing its volume. The volume of the chamber thus moves between a minimum value of 16 liters (before dust dispersion) to a maximum value of 21.6 liters (at the moment of the rupture of this membrane). When the suspension is triggered to perform the deflagration, this deformable membrane behaves as a rupture disk, avoiding the achievement of excessively high overpressure. The disk is characterized by low resistance to minimize the disturbance of the flame at the moment of rupture of the disk. The rupture of the disc occurs at about 35 mbar, as measured in some preliminary tests.

This means that the disturbance of flame propagation is minimized.

Two kind of tests can be performed. Dispersion tests allow the characterization of the dust cloud produced; for these tests no ignition of the dust cloud is realized. Flame propagation tests allow the visualization of the aluminum dust flame propagation in the prototype.

A dispersion test consists in the following stages: the powder is weighed and placed in the appropriate tanks. The pressure inside the air tanks reaches the desired value. The solenoid valves open and remain open for a set time. The air flows up to the dust, raises it and the flow of air and dust undergoes pre-mixing. The flow continues inside the injection tubes; through the series of holes, it enters the chamber. At the end of each test, the powder remaining in the tanks is weighed, and the amount of powder injected is defined.

The flame propagation test is carried out in the following phases. First, dust is injected in the prototype as previously described. After an adjustable time delay between the end of the suspension and the ignition, the electric arc is generated, and the mixture ignites. During the propagation of the flame, the rupture disk opens.

1.3 Physical measurements

1.3.1 Dispersion test

For each dispersion test, the total volume of the prototype has to be determined at the end of the injection process (membrane swelling). For this purpose, two sensors (temperature sensor, and pressure sensor) are positioned inside the air vessels. The temperature sensor is a 1mm-diameter thermocouple (T type). The pressure sensor is a membrane sensor with a maximal pressure of 40 bar. Another thermocouple identical to the previous one is positioned inside the prototype. The evaluation with these sensors of

the total volume at the end of dust injection will be explained in Chapter 3.

1.3.2 Flame propagation test

For flame propagation tests, two piezoelectric PCB sensors are used. The first one is located at 15 cm from the bottom of the prototype. It sensitivity is 6 939,6 mbar/V. A second one is located at 9 cm below the rupture disc, its sensitivity is 691,6 mbar/V. Data of both sensors are recorded at a frequency of 200 kHz. Results obtained with both sensors are fairly close. In this manuscript, only data obtained from the upper sensor are exposed, as this sensor is more sensitive.

2. Optical methods

2.1 Concentration measurement using MIE scattering

The global concentration is calculated dividing the mass of powder injected by the confinement volume. It is necessary to verify that the powder is distributed homogeneously in the volume of the prototype at the moment of ignition. In fact, strong concentration gradients in the suspension influence the propagation of the flame inside it. The homogeneity of the suspension is investigated performing MIE scattering, by testing various dust concentrations and different dispersion configurations.

2.1.1 Method presentation

This method is based on the MIE scattering phenomenon: when a light source illuminates particles inside the flow, the particles diffuse the light in all the directions. The intensity of the scattered light is therefore proportional to the number of particles that scatter the light.

The Figure 20 schematizes the measurement method.

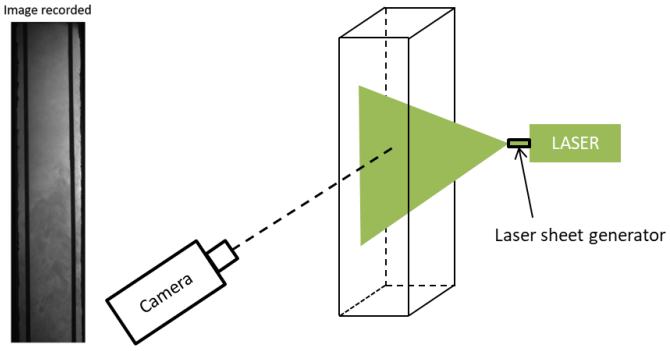

Figure 20: Experimental set up of MIE scattering

A laser sheet illuminates a plane of the flow. The particles present in this plane will then diffuse the light in all the directions. A camera placed at 90 ° to the laser plane collects

the light scattered by the particles.

In the images obtained, the gray levels refer to the number of particles present in each part of the luminous plane. In particular, the luminous areas correspond to the high concentration areas and the dark ones to the low concentration areas. Therefore, this method allows obtaining the degree of homogeneity of the suspension formed in a plane of the flow, without disturbing the flow itself. However, the technique does not allow to obtain the local value of particles concentration. This technique gives information about the homogeneity level inside the suspension and permits to calculate the local concentration relative to the average value in the plane of the flow.

2.1.2 Image analysis

In each MIE scattering test, the camera records a sequence of images which shows the evolution of the homogeneity of the suspension. The images obtained in the tests shall be treated in order to establish the link between the recorded luminous intensity and the homogeneity of the suspension. For this purpose, these images have to be corrected as their grey levels are not directly proportional to the homogeneity degree.

The first correction is made considering what is recorded by the camera when the prototype is empty of dust; indeed when the laser illuminates the empty prototype, some areas may be brighter due to unwanted reflections. An acquisition is then carried out under these conditions, obtaining an image called I_0, represented in Figure 21 (left).

Furthermore, the power variation of the laser sheet must be taken into account: even in the presence of a homogeneous suspension, the central part will be brighter than the extremities. A second preliminary acquisition is then performed; the prototype is filled with a smoke suspension illuminated by the laser plane. The image obtained is called I_{bg} , represented in Figure 21 (right).

The raw image (I) is then corrected by applying the following relationship:

$$I_2 = \frac{I - I_0}{I_{bg}}$$

I_2 is the grayscale matrix of the corrected image.

Figure 21: I_0 image on the left, I_{bg} on the right

The second correction takes into account the attenuation of the laser light in the passage through the suspension of particles. Considering I_{laser}, the intensity of the incident laser, d, the distance between the incidence point of the laser and any point (x, y) inside the suspension, an attenuation coefficient K, the light attenuation can be calculated using the Beer-Lambert law:

$$I_3(x, y) = I_{laser} * e^{-K*d}$$

For each point (x, y) in the suspension, this correction is considered, obtaining the I_3 matrix of the corrected image.

The value of K must be determined for each concentration of powder introduced. To determine this coefficient, from all the tests realized with a same dust concentration, an ensemble mean image is calculated from all the images I_2 of the individual tests. For all the pixels, defined by its coordinates (x, y), a reference pixel is defined. A laser beam

gets to each pixel (x, y): the reference point for each pixel corresponds to the entry point of the laser beam, passing through the pixel itself. The distance traveled by the laser beam inside this dust cloud (d) is also determined, considering the divergence of the laser sheet. These notations are represented in Figure 22. With this image I_2 and the intensity of the corresponding pixel of reference (I_{ref}), the value of K is obtained through a linear regression:

$$\ln\left(\frac{I_2}{I_{ref}}\right) = -K * d$$

After this determination of the coefficient K, the images corrected I_3 are obtained thanks to the previous Beer-Lambert law.

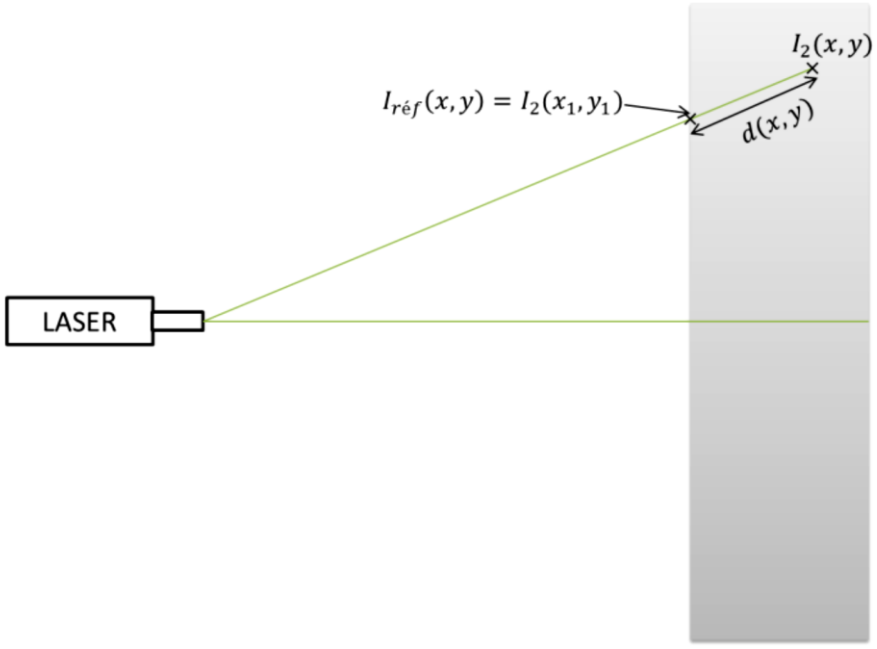

Figure 22: Laser plane divergence, representation of the notations

The final step allows obtaining the 2d maps of the homogeneity degree of the suspension. To do this, I_3 is normalized respect to an average value, $\overline{I_3}$, which is the spatial mean of each image I_3. Each element of I_3 is then divided by $\overline{I_3}$, obtaining a new

matrix that is called I_{final}.

I_{final} represents the distribution of dust concentration in the prototype, giving information on the homogeneity of the dust cloud. A color map of this matrix is shown in Figure 23, where the corresponding raw image captured by the camera is also represented. In the image after analysis (on the right), the red areas correspond to homogeneity degree superior to 1. These red parts are therefore more concentrated areas. On the contrary, blue areas correspond to less concentrated areas.

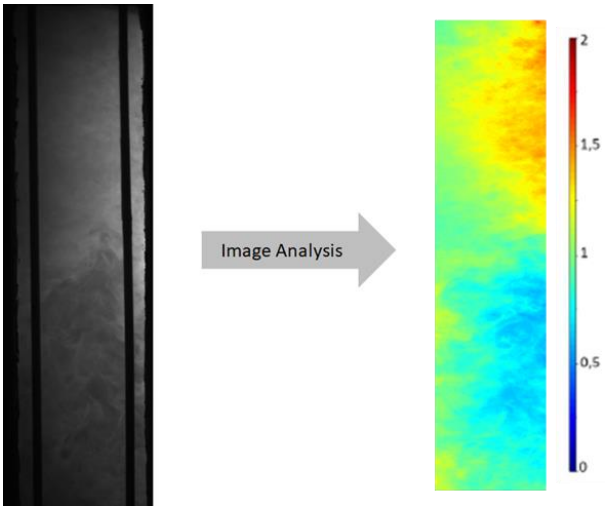

Figure 23: raw image of the suspension on the left, color map of the suspension on the right

2.2 Turbulence measurement using Particle Image Velocimetry (PIV)

The PIV technique is a non-intrusive measurement of flow velocity, characterized by a high spatial resolution. This technique allows obtaining 2D maps of the flow velocity and their evolution over time.

2.2.1 Method presentation

In order to determine the velocity field, the PIV technique requires the presence of

tracers within the flow. In the case of dust-air suspensions, the particles themselves act as tracers.

A laser plane illuminates the suspension and the light scattered by the particles is captured by a camera placed at 90° to the laser plane. In this way, the position of the dust is immortalized, and comparing two consecutive images, the velocity can be deduced.

The PIV scheme is shown in Figure 24.

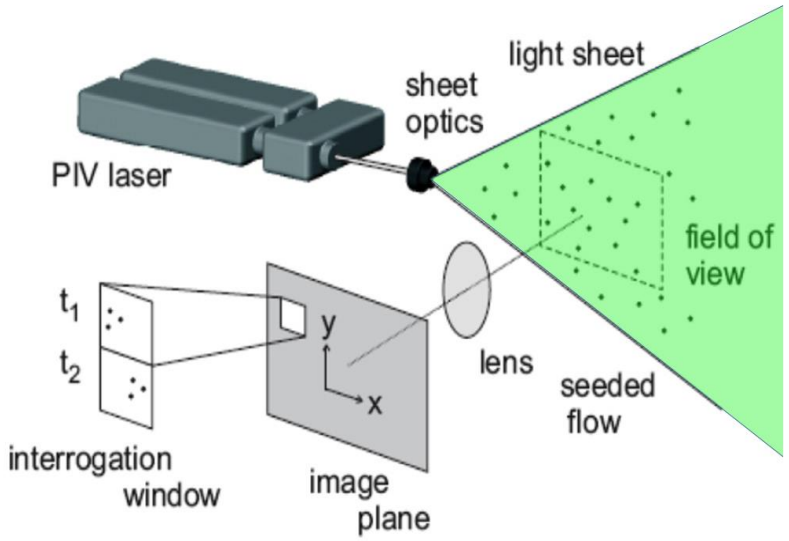

Figure 24: PIV scheme (Xu et al. 2017)

The sequence of image pairs can be obtained in two ways:

With a high speed camera and a continuous laser; in this case, the time interval between two images is set by the camera acquisition sequence.

With a slow camera synchronized with a pulse laser; in this case, the time interval between two images is equal to the time between the two laser pulses.

Between two successive images, the velocity vectors are constructed by dividing each

image into interrogation areas. The interrogation areas of two consecutive images are then compared: within each interrogation area, a spatial intercorrelation calculation estimates the most probable displacement of the particles. The velocity vector is then calculated in each interrogation area dividing the displacement by the delay time between the two images. At the end, a detailed velocity vectors map is generated.
The 2D velocity maps are obtained using the DynamicStudio software, developed by Dantec Dynamics. The software uses an adaptive PIV method; this means that the size and shape of the interrogation areas are not constant, but are adjusted depending on the image. The interrogation areas are drawn considering the presence of particles and velocity gradients within the flow. The range of variation of the interrogation area is chosen to be between 8 and 32 pixels.

To obtain satisfactory results from a PIV measurement, the values of two related parameters have to be carefully chosen: the delay time between two images and the size of the interrogation area. These parameters depend on the flow characteristics. The combination of these two factors must ensure that the displacement of the particles between one image and the next is between ½ and ¼ of the interrogation area.

2.2.2 Image analysis

The method allows the measurement of instantaneous velocity U. To obtain turbulence intensity we shall calculate the fluctuating component of velocity, $'$. The latter can be determined from the measured values of U by defining an average velocity ($\overline{U}$), as previously mentioned in Chapter 2.
Due to the highly transient nature of the flow, a temporal average of instantaneous velocity values seems not adequate. An ensemble average at each instant is preferred, calculated by doing a mean between the instantaneous velocity values of numerous tests (Wang et al. 2006) (Hosseinzadeh et al. 2018)

As previously mentioned, the software generates a map of the velocity vectors for each test for different instants; each vector of the map corresponds to an interrogation area. For each velocity vector U the software returns the values of its horizontal (u) and vertical (v) components, as shown in Figure 25. The bond between the vectors and the interrogation areas is highlighted.

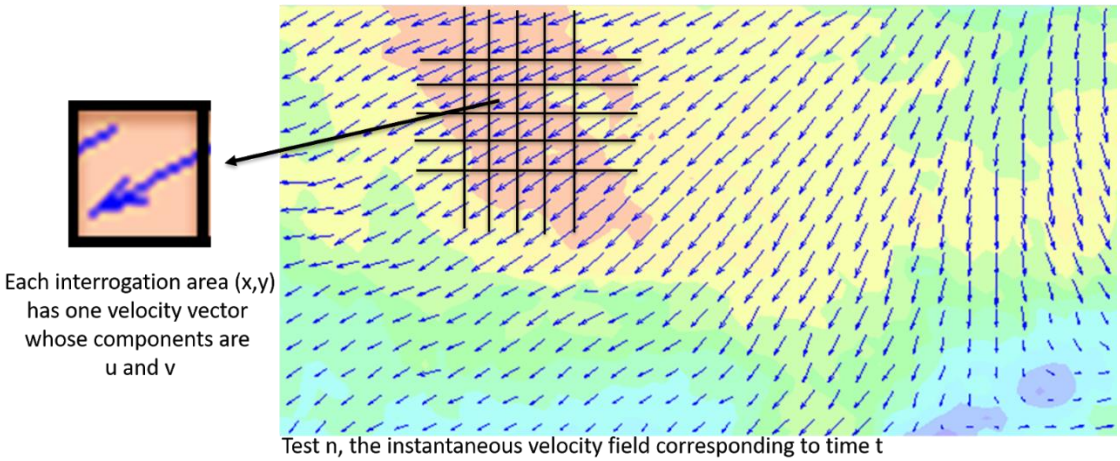

Figure 25: Color map of velocity field, with the representation of interrogation areas

The average components of the velocity $(\bar{u}, \bar{v})$are calculated using the following relationships:

$$\bar{u}(x,y,t) = \frac{1}{n}\sum_{i=1}^{n} u_i(x,y,t)$$

$$\bar{v}(x,y,t) = \frac{1}{n}\sum_{i=1}^{n} v_i(x,y,t)$$

n corresponds to the number of tests performed and (x,y) are the coordinates of the center of the interrogation area.

The velocity fluctuation components (u', v') are then calculated using the Reynolds decomposition:

$$u'(x,y,t) = \frac{1}{n}\sum_{i=1}^{n}\left(u_i(x,y,t) - \bar{u}(x,y,t)\right)^2$$

$$v'(x,y,t) = \frac{1}{n}\sum_{i=1}^{n}\left(v_i(x,y,t) - \bar{v}(x,y,t)\right)^2$$

The turbulence intensity is obtained with the following equation:

$$IT(x,y,t) = \sqrt{u'(x,y,t) + v'(x,y,t)}$$

$IT(x,y,t)$ represents the value of turbulence intensity in each interrogation area (x,y) of the image recorded, at a specific time (t).

Two parameters are important as they influence the turbulence results. First of all, as the mean velocity is determined by an ensemble-averaging over all the tests realized, the number of tests is a first important parameter. Furthermore, the size of the field of view is linked to the size of the eddies measurable by the PIV algorithm. Thus, also this parameter influences the turbulence results. The importance of these parameters will be highlighted in Chapter 3. The experiments realized and the results obtained to estimate these two parameters are also exposed in Chapter 3.

2.3 Turbulence measurement using Laser Doppler Anemometer (LDA)

The Laser Doppler Anemometry (LDA) is a non-intrusive technique that allows measuring the local velocity of the particles within a flow, with a high temporal resolution.

2.3.1 Method presentation

As the optical techniques analyzed previously, the LDA is also based on the principle of light dispersion when a light source illuminates solid particles. This technique uses this principle coupled with the Doppler effect. The special feature of the LDA consists in measuring the difference between the frequency of the light that illuminates the particles and the frequency of the light dispersed by the particles. This frequency

difference is called "Doppler shift frequency" and is directly related to the particle velocity, according to the following relationship:

$$f_D = \frac{\vec{V}}{\lambda}\left(\overrightarrow{u_1} - \overrightarrow{u_2}\right)$$

Where f_D is the Doppler frequency, $\vec{V}$ is the flow velocity, λ is the wavelength of the incident light, $\overrightarrow{u_1}$ is the propagation direction of the incident ray, $\overrightarrow{u_2}$ is the observation direction.

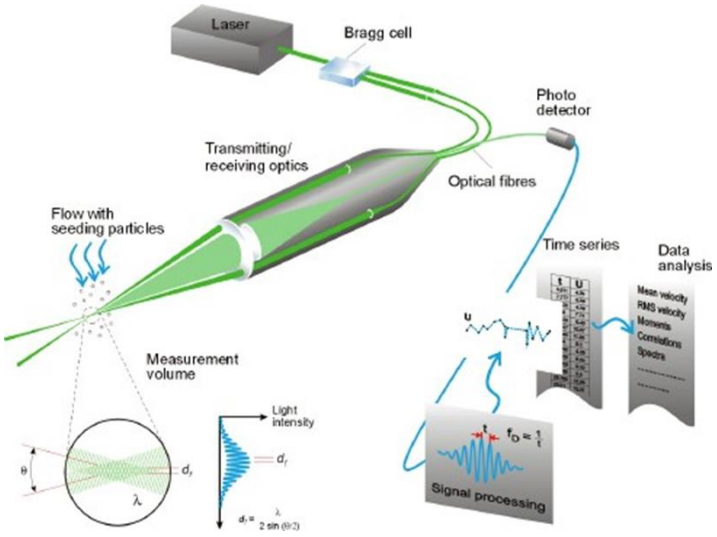

Figure 26: LDA scheme (www.dantecdynamics.com)

The experimental apparatus used to carry out this measurement is shown in Figure 26. A Bragg cell divides a laser beam into two beams of the same intensity. An optical transmitter deflects the laser beams so that they intersect in a zone called "measurement volume"; this corresponds to the volume of the flow where the local velocity value is measured. This figure also shows the evolution of light intensity within the measurement volume: interference fringes are distinguishable. The interference distance (d_f) is calculated using the following formula:

$$d_f = \frac{\lambda}{2sin\left(\frac{\theta}{2}\right)}$$

θ is the angle between the laser beams.

When a particle moving in the fluid passes through the measurement volume, the light diffused by the particle is collected by the receiving optics and transmitted to the photodetector, as shown in Figure 26. The photodetector produces a signal at the Doppler frequency f_D. The velocity is then calculated with the following equation:

$$v = d_f * f_D$$

In Figure 26, the experimental apparatus uses only one laser source. One laser source allows measuring one component of the velocity vector. The other components of the velocity vector can be calculated using multiple laser sources. The Figure 27 shows the LDA measurements performed by Bozier in his experimental work (Bozier 2004): the photo shows the prototype interior seen from above, where the laser beams intersect for the three-dimensional measurement of velocity. Three laser sources are used: blue and green laser beams crossing the prototype horizontally, violet laser beams crossing the prototype vertically.

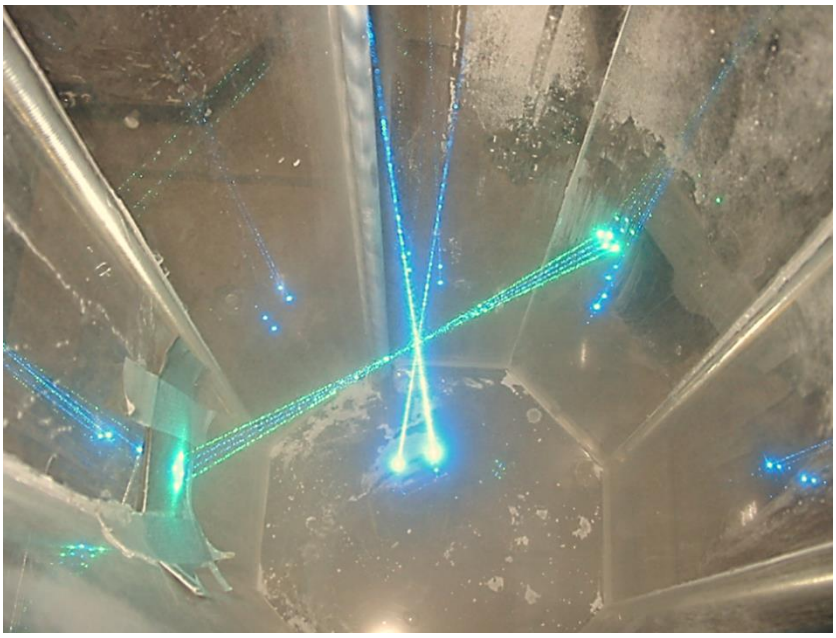

Figure 27: laser beams intersection inside Bozier prototype (Bozier 2004)

2.3.2 Data analysis

As previously explained for the measurement of turbulence with the PIV technique, also in the case of the LDA an average velocity has to be calculated. From the latter, the fluctuating component is obtained, and therefore the turbulence intensity. In the case of the LDA, thanks to the high temporal resolution of this technique, the average velocity is generally calculated through a time averaging.

As it will be shown in Chapter 3, the studied flow presents a null mean velocity. For this reason, for LDA analysis, the mean flow is considered equals to zero. From this null mean velocity and the instantaneous velocity obtained by PIV, turbulence intensity can be evaluated with the method presented hereafter. A temporal average is used to obtain turbulence intensity data averaged on time intervals (whose length is Δt). This temporal averaging, coupled with ensemble averaging from the different tests realized, allows reducing the number of tests realized to obtain turbulence intensity data.

The analysis method is as follow. First, the components of the fluctuating velocity in each Δt interval are calculated considering a null mean velocity:

$$u'_n|_{\Delta t} = \frac{1}{N_{data}} \sum_{i=1}^{N_{data}} u_n(t_i)^2$$

N_{data} is the number of data acquired in the time window Δt (corresponding to the number of particles that passed through the measurement volume and whose speed was measured). The subscript n indicates the nth test. $u_n(t_i)$ is the velocity values acquired by the LDA (in the nth test and corresponding to the instant t_i) and $u'_n|_{\Delta t}$ is the fluctuating velocity value measured in the Δt interval of the nth test.

Subsequently, the ensemble average of the fluctuation values, obtained for each Δt interval, based on the number of tests is carried out:

$$u'|_{\Delta t} = \frac{1}{N} \sum_{i=1}^{N} u'_i|_{\Delta t}$$

$u'|_{\Delta t}$ represents the average fluctuation in the Δt interval within the studied flow over the N tests realized.

From this value the turbulence intensity (IT) is calculated:

$$IT|_{\Delta t} = \sqrt{u'|_{\Delta t} + v'|_{\Delta t}}$$

(if the LDA measurement is 2 components)

The choice of Δt is delicate. A too short Δt leads to an overestimation of turbulence intensity (every fluctuation Is considered as turbulence); on the contrary, a too long interval of time implies an underestimation of the turbulence intensity.

The analysis of the LDA signal through the Fast Fourier Transform (FFT) is used to obtain a coherent value of Δt. The LDA data are non-equidistant as each data is captured only when a particle passes through the measurement volume. For this reason, the resampling of the data is realized. Then the Fourier transform of this resampled signal is calculated. Figure 28 exposes an example of Fourier transform result. A first minimum is observed for a frequency around 13 Hz, corresponding to a time interval of 77 ms. A time interval of 80 ms is thus used in this study for the LDA data analysis.

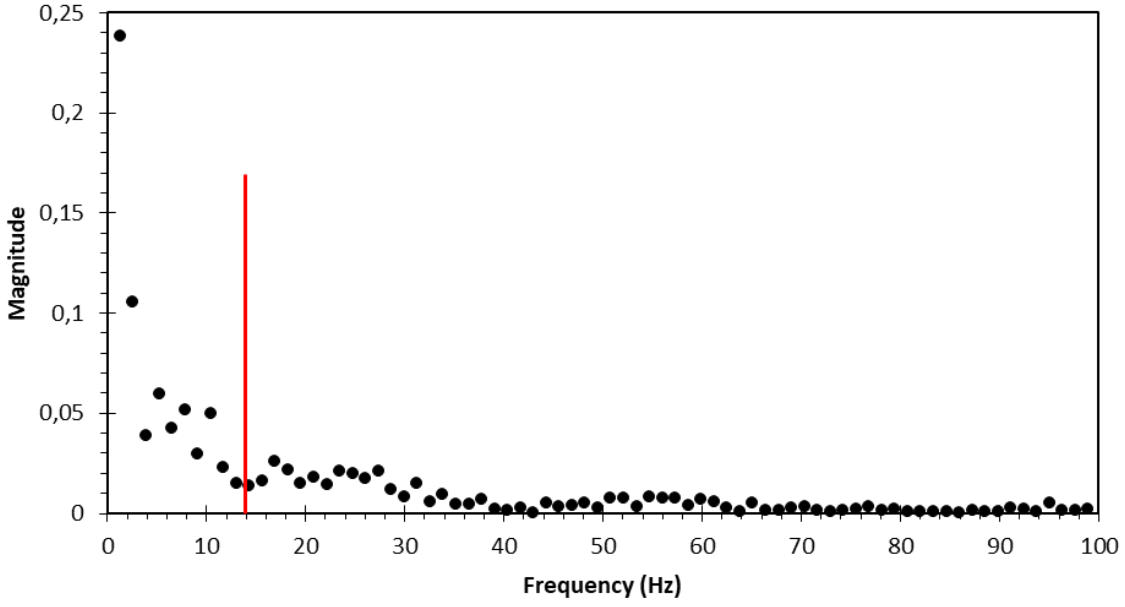

Figure 28: Example of Fourier transform of LDA data

2.4 Visualization of flame propagation: direct visualization

Flame propagation is recorded by a high-speed camera and pressure sensors. The pressure sensors characteristics have already been detailed in part 1.3.1. The high-speed camera records the light emitted by the flame; this technique is called direct visualization. The flame front position is determined with the images obtained; then flame velocity is evaluated. The flame front position is determined thanks to an algorithm based on thresholds. The high-speed camera and the pressure sensors are synchronized; thus the results obtained at the same instant with both techniques can be compared.

For this study, a Photron SA3 high-speed camera is used, equipped with a 17-35 mm lens. The lens aperture is chosen to be f/22. A frequency of 7500 fps (frames per second) and a resolution of 1024 x 256 pixels are fixed. Exposure time is set to 2 μs. These optical parameters are chosen to obtain non-saturated images during the propagation of the flame front inside the visualization section of the prototype. Some problems encountered while analyzing saturated images have been emphasized in (Chanut et al., 2018).

Chapter 3

Results

1. Study of dust concentration homogeneity

Dust concentration results are presented in this part. First, a focus on the dispersion system is realized: determination of the total volume at the end of injection, conditions for the rupture of the membrane and repeatability of the tests in terms of mass injected. Then, the results of Mie scattering in terms of concentration homogeneity are exposed. The results analysis is carried out following two main stages: first, the evolution of homogeneity is investigated on a single test, performed injecting a certain dust concentration and by choosing a defined dispersion configuration. Finally, the evolution of the homogeneity level of the dispersion with variations in dispersion configurations is investigated.

1.1 Focus on the dispersion system

As previously mentioned, the dispersion system releases pressurized air into the injection tubes. The air raises the dust placed in a specific area of the tubes, and the suspension enters the prototype. On top of the prototype, a deformable membrane is located. This element maintains confinement for the suspension during the dust injection process and avoids a significant pressure rise inside the chamber during the flame propagation. Therefore, the volume of confinement changes as the suspension is introduced into the prototype, as illustrated in Figure 29.

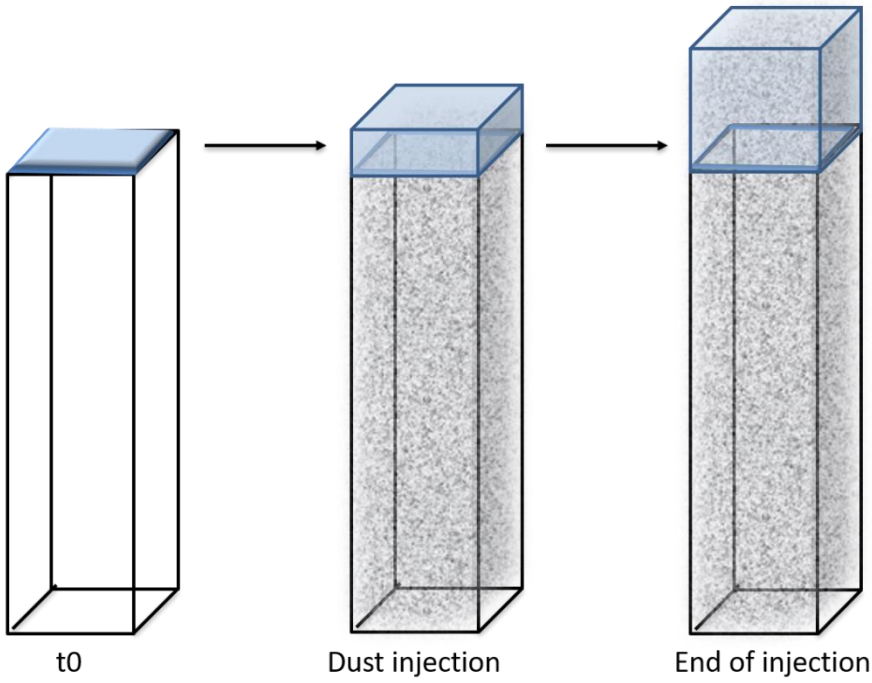

Figure 29: Membrane expansion during the injection of the suspension

The concentration of powder introduced can only be calculated if the confinement volume reached at the end of the dispersion is known. The volume calculation is carried out in the following way. During the injection, temperature and pressure inside the air tanks are recorded. The volume of the air tanks is known. Inside the prototype, the temperature is measured as well (see Chapter 2). Through a material balance the change in volume inside the prototype due to air introduction is determined:

$$\Delta V = \frac{T_{pro}}{P_{pro}} * \left(\frac{P_f * V_R}{T_f} - \frac{P_0 * V_R}{T_0} \right)$$

Where T_{pro} and P_{pro} are the temperature and the pressure (atmospheric pressure) inside the prototype respectively. P_0 and P_f are the initial and final pressures inside the compressed air tanks. T_0 and T_f are the initial and final temperatures inside the air tanks. V_R is the total volume of the air tanks.

The dispersion configuration is characterized by two main parameters: the pressure inside the air tanks (at which air is discharged), and the injection time (starting and

ending with the opening and closure of the solenoid valves respectively). For each chosen dispersion configuration, the final volume of the prototype is calculated at the end of the injection, thus allowing the determination of the particle concentration. For example, choosing an initial pressure of 2.5 bar and an injection time of 800 ms, the volume variation has been measured to be 2.4 L.

Tests were carried out to determine the maximum volume of the membrane. For a chosen value of pressure in the air tanks, tests were performed at various injection time: the aim was to find the time at which the membrane passes from the condition of maximum extension to breakage. With an initial pressure of 4 bar inside the air tanks, the membrane does not break if the valves are open for 0.9 sec; the rupture happens after 1 sec. The maximum volume of the membrane was therefore found between 5.1 and 5.4 L.

For deflagration tests, the membrane has to be intact when the mixture is ignited: this ensures the initial confinement of the suspension and allows calculating the concentration at the moment of ignition. For this reason, a preliminary study was carried out on different dispersion configurations. The aim of these tests was to find different combinations of air pressure and injection time which gave the rupture of the membrane. The results of this preliminary study are summarized in the Table 2. With this table, the limit conditions of the injection process are exposed

Table 2: Study on different dispersion configurations

Pression in the air vessels (bar)	**Injection time (s)**	**Membrane rupture**	**Variation of confinement volume (L)**
4	0.9	no	5.1
4	1	yes	5.4
5	0.4	no	4.7
5	0.5	yes	5.6
6	0.3	no	4.6
6	0.4	yes	6

Numerous tests were performed by injecting different masses of powder in a same injection configuration (2.5 bar pressure in the air tanks and 800 ms injection time). The reproducibility in terms of concentration between different tests is shown in Table 3. For each tested mass, many tests have been carried out: a mean concentration on the tests has been measured, as well as a standard deviation between the different tests. Moreover, the values of standard deviation and mean concentration have been compared. The ratio between these two quantities gives information about the reproducibility of the dust injection process. This ratio is less than 10% for each configuration.

Table 3: Reproducibility in terms of concentration as a function of the initial mass. The mean and the standard deviation are on several tests performed at 2.5 bar (pressure in air tanks) and 800 ms (injection time)

Initial mass (g)	**Mean Concentration (g/m^3)**	**Standard Deviation of the concentration (g/m^3)**	**Ratio (standard deviation/mean concentration)**
6	183	10	5%
6.8	225	14	6%
8	273	24	9%
10	361	27	7%

The Figure 30 shows images obtained by MIE scattering. The images are relative to a test carried out by injecting air at 2.5 bar and whose injection lasted 800 ms. The times below each image in the sequence correspond to the time after the start of the injection. The suspension in the first moments is characterized by strong turbulence and is located mainly in the center of the prototype. At the instant t = 800ms, the solenoid valves are closed. After the end of the injection, the suspension seems stationary and becomes more and more homogeneous.

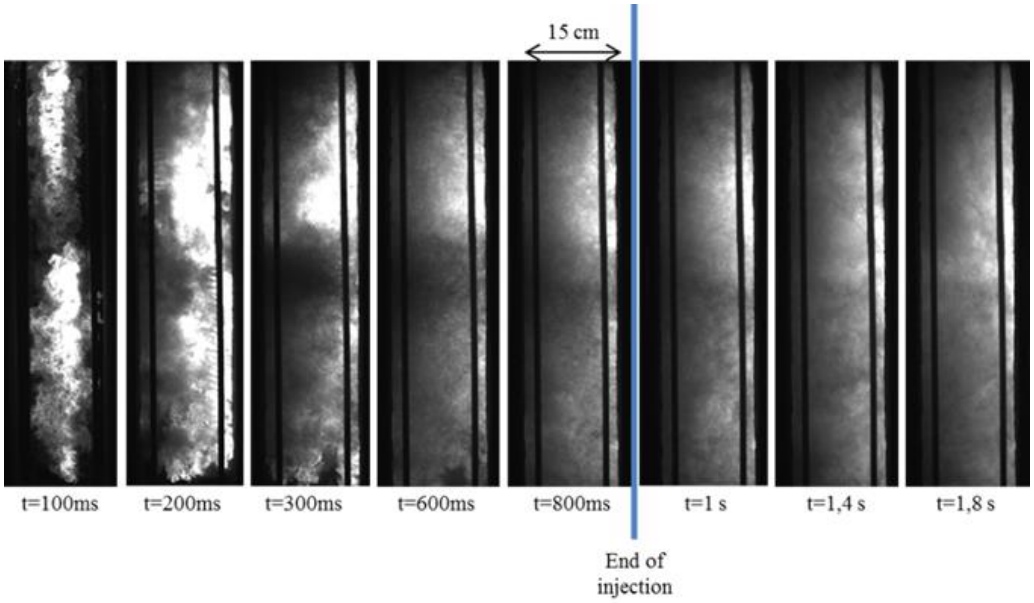

Figure 30: Dispersion stages (2,5bar, 800ms injection) , MIE scattering images

In the subsequent parts of this chapter, the initial time ($t_0 = 0$ ms) will no longer be taken at the opening of the solenoid valves but will correspond to the moment of their closure. Indeed, the ignition of the dust suspension will happen after the end of the dispersion. Thus, the dust dispersion process is only analyzed after the closure of the valves.

1.2 Presentation of the tests

The experimental set up of MIE scattering tests is shown in Figure 31.

A LITRON pulsed Nd: YAG laser (200 mJ / 15 Hz) is used coupled to a laser sheet generator. The laser is used in single pulse mode, with a 100 ms delay between pulses. Its wavelength is 532 nm. The laser sheet passes through the center of the prototype along its entire height.

Figure 31 shows that the suspension is studied in an area between 3.5 cm and 66 cm from the base of the prototype, which corresponds to almost 90% of the total height of the prototype. The laser power was too weak at the extremities of the prototype to allow the study of homogeneity in those parts.

A Hamamatsu HiSense camera is used, with a 17-35 mm lens and an aperture sets to f / 4. The resolution is 2048x2048 pixels, with a frequency of 10 fps (frames per second). The exposure time is chosen to be 66.9 μs.

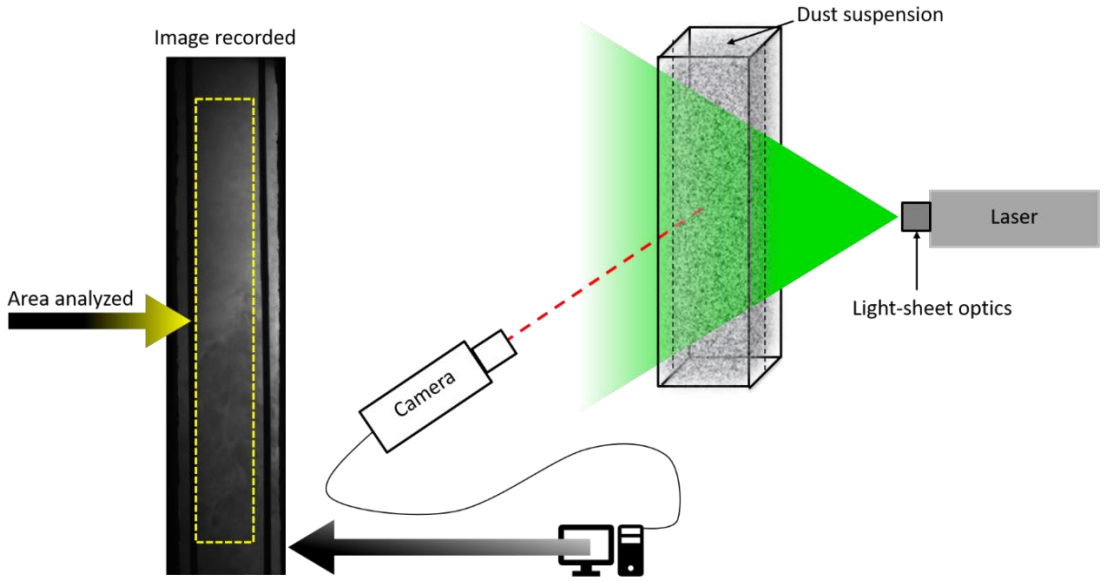

Figure 31: Experimental set up of MIE scattering

Two dispersion configurations have been analyzed: 2.5b/800ms and 4b/300ms (initial pressure in the air tanks/injection time). With these two configurations, the same quantity of air is injected inside the prototype.

For each experimental configuration (initial mass, initial pressure in the air tanks, injection time), at least 5 tests were performed. For each test, the images obtained were processed numerically as presented in Chapter 2. At the end, an average image is obtained from these 5 tests. All the results presented in this section concern these average images.

1.3 Evolution of the concentration homogeneity

An example of results of the study of the suspension homogeneity in terms of concentration is presented in Figure 32. The figure shows the evolution of the homogeneity of the suspension obtained by inserting an initial mass of 1.7 g of aluminum in each injection tube. The dispersion configuration is as follows: 2.5 bar as initial pressure in the air tanks and 800 ms as injection time. This figure shows the images obtained before and after digital processing.

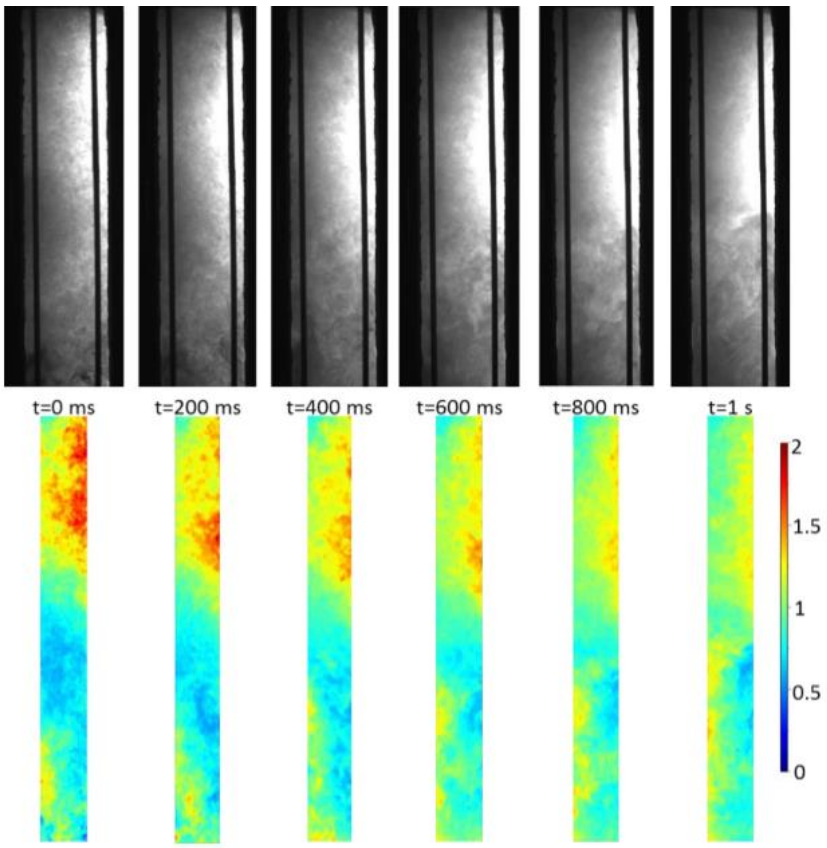

Figure 32: Evolution of homogeneity over time (2.5b/800ms)

The colormaps are relative to the local homogeneity degree. It is a non-dimensional data as it has been divided by the mean value of the luminous intensity recorded in each image (spatial average). According to the MIE scattering theory, the brightest areas of

the greyscale images correspond to more concentrated suspension zones; in the colormaps, these areas are red. The homogeneous zones, in which the concentration of the suspension is close to the average value, correspond to the green parts on the colormaps. In the case of a perfectly homogeneous suspension, the colormap should be all green (value of 1).

After the end of the injection ($t = 0\ ms$), the mixture is not very homogeneous: the upper part of the prototype is more concentrated. Over time the mixture seems instead to become more and more homogeneous.

Figure 33 shows the evolution of the homogeneity level over time: the graph has the dimensionless luminous intensity on the x-axis and the height of the prototype on the y-axis. Spatial mean is calculated for each line of pixels, corresponding to different heights. The level of homogeneity of the suspension along the vertical axis of the prototype has a profound influence on flame propagation. Indeed, high concentration gradients along the direction of propagation can disturb this propagation. The dispersion system of this prototype was built to obtain the best homogeneity along this axis. After some analysis, an objective of global homogeneity of 20% has been chosen; it seemed too complicated to obtain a cloud more homogeneous. This 20% criterion for the deviation of the dimensionless luminous intensity is represented by the red vertical lines in Figure 33.

In the first moments (after the end of the injection) the suspension is not homogeneous, with a dimensionless luminous intensity deviation in some parts of the prototype greater than 20%. From 0.6 sec after the end of the injection, the luminous intensity values of the suspension fall within this desired interval.

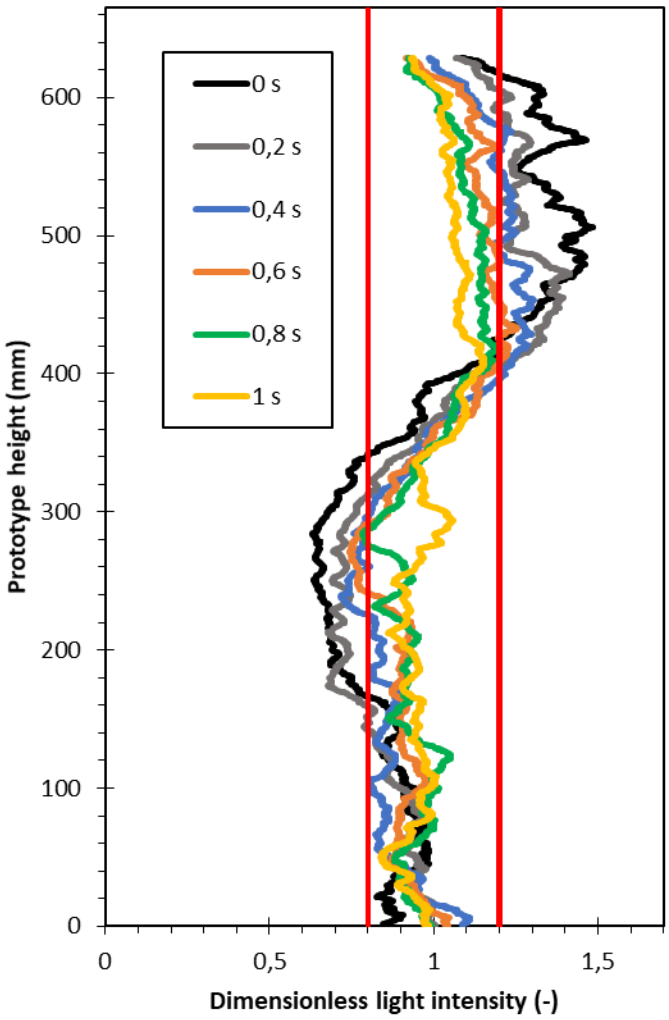

Figure 33: Evolution of homogeneity over time along the height of the prototype

For the same dispersion configuration (2.5bar / 800ms), numerous tests were performed at various concentrations of powder initially introduced. Results were similar (suspension homogeneous along the height of the prototype after a delay of around 600 ms) in the case of masses inserted in each tube equal to 2.5 g, 2 g, and 1.7 g.

For values higher than 2.5g the method is not adequate as the high quantities of dust introduced create deposits on the walls of the prototype, thus preventing optical access to the phenomenon. For values below 1.7 g, the few particles present in the prototype do not give a sufficient scattering effect.

In order to study how dispersion (in terms of homogeneity and turbulence) influences flame propagation, a dispersion configuration other than 2.5bar / 800ms has also been analyzed: the 4 bar / 300 ms configuration is chosen. The air introduced in the two cases is calculated to be the same. The choice derived, as we will see later, from the differences in the levels of turbulence induced in the suspension relative to these two configurations.

In this part, the comparison between the results of the tests performed in the two configurations is presented. In Figure 34, evolution over time of the homogeneity of the suspension along the height of the prototype for both dispersion configurations is exposed. The red vertical lines represent the desired interval of the dimensionless luminous intensity (+/- 20%). In the case of 2.5 bar / 800 ms, the suspension respects this criterion after 0.5 sec from the end of the injection; for the 4 bar / 300 ms configuration, after at least 0.7 seconds.

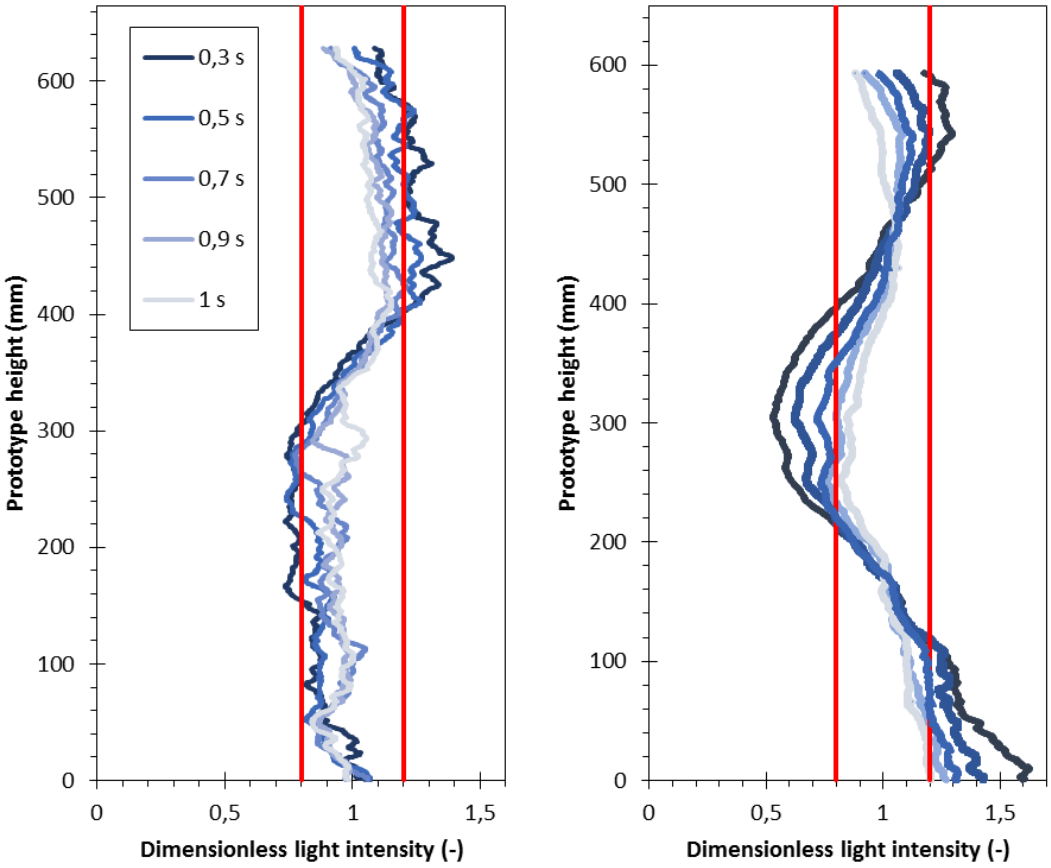

Figure 34: Evolution of homogeneity over time along the height of the prototype 2.5/800ms (left), 4b/300ms (right)

The results of this comparison are also reported in Figure 35. Here the evolution of the standard deviation of the dimensionless luminous intensity is represented for both dispersion configurations (2.5bar / 800ms, 4bar / 300ms). The spatial standard deviation is used, as the spatial mean value is always 1; the images being normalized by the spatial mean. As already mentioned, the objective of the study is to observe at which time from the end of the injection the standard deviations of luminous intensity decrease below 20%. The red horizontal line in the figure represents this criterion. By waiting longer time the homogeneity improves for both configurations; a delay of at least 0.7 sec for both configurations is necessary to fall below the limit value.

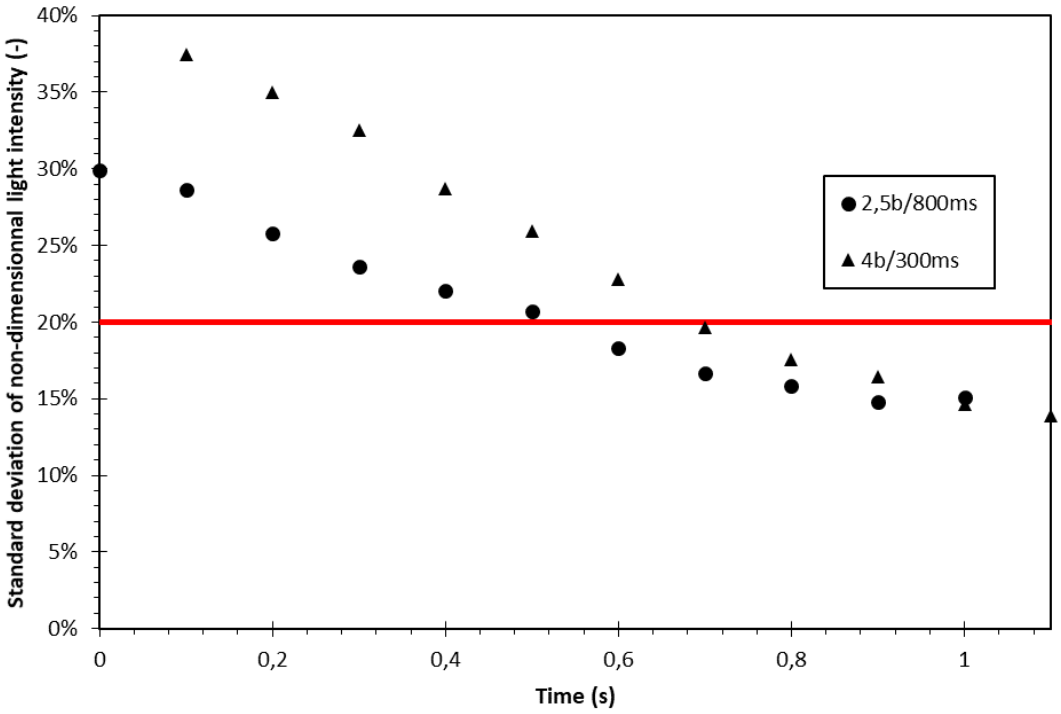

Figure 35: Evolution of standard deviation of non-dimensional light intensity over time, for both dispersion configuration

1.4 Conclusions

MIE scattering tests have been carried out, for numerous concentrations and in different dispersion configurations. When the suspension is obtained at 2.5 bar / 800ms the levels of homogeneity in the whole prototype become acceptable after around 0.6 sec from the end of the injection; in the case of 4bar / 300ms dispersion configuration, after around 0.7 sec

The study of the concentration and the comparison between different dispersion configurations is important in order to choose the suspension ignition time in the subsequent flame propagation tests. This choice can be made only by having results available on the level of turbulence of the suspension and its evolution over time. For this reason in the next part results about dispersion-induced turbulence will be presented.

2. Study of dispersion-induced turbulence

In this part, turbulence level is studied within the flow.

A preliminary study has been carried out in order to optimize the experimental conditions to perform the PIV measurements and to define the minimum number of tests required for this analysis.

Subsequently, the turbulence level inside the suspension is analyzed with two complementary optical methods: PIV and LDA. Two dispersion configurations have been studied.

2.1 Preliminary study: optimization of PIV measurements

2.1.1 Presentation of the study

The PIV measurement allows observing the turbulence of the flow in terms of turbulent structures carrying kinetic energy. To investigate these structures, PIV cannot be used over the entire height of the prototype. Indeed with a too large field of view (measurement zone), because of the limited resolution of the images, only global flow movement is recorded; all the eddies carrying kinetic energy cannot be measured, and thus turbulence intensity is under estimated. An original study is carried out in order to understand which field of view allows performing PIV in the best conditions, which is based on multiscale PIV measurements.

As previously mentioned in Chapter 2, for PIV analysis, mean flow velocity is calculated based on an ensemble-averaging over all the tests realized under the same conditions. The number of tests performed thus influences the results of turbulence intensity. This preliminary study also allows defining the minimum number of tests realized to obtain coherent turbulent intensity results.

2.1.2 Tests presentation

The tests of multiscale PIV consist of simultaneously recording on several cameras the turbulence level of the dust suspension. All cameras look to the same area of the flow and are focused on the laser plane used for the PIV. However, each camera has a different size of field of view. In this way, by analyzing the results, the differences in terms of turbulence intensity recorded by the three cameras can be quantified. Therefore, the size of PIV field of view used in subsequent tests can be chosen.

The multiscale PIV of this study investigated three different sizes for the PIV field of view. In the zone of the flow investigated with PIV multiscale, LDA (2 components) was also performed. Figure 36 shows a schematic representation of the setup of this preliminary study.

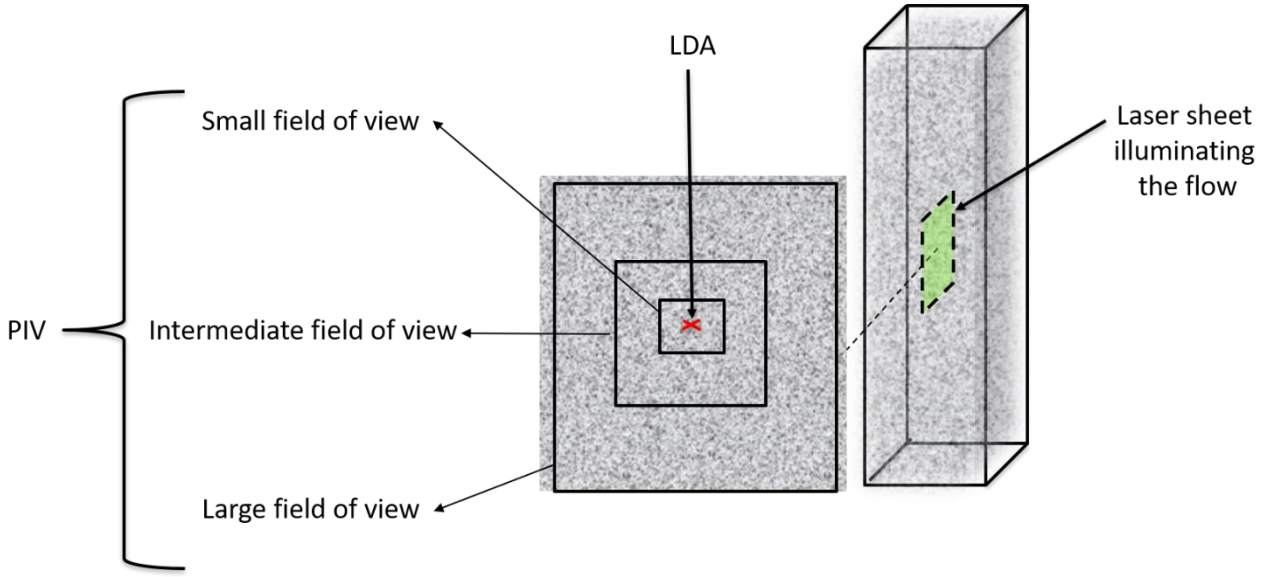

Figure 36: Schematic representation of experimental setup to perform PIV multiscale and LDA

For these three simultaneous PIV measurements, in addition to the continuous laser, three high speed cameras were needed.

For the large field of view of study, with a size of 10 cmx10 cm, a Photron SA3 camera was used, equipped with a lens with a fixed focal length of 105 mm, coupled with a focal doubling system. The lens aperture is set at f / 2.8. The resolution of this camera is 1024x1024 pixels, with a chosen frequency of 1000 fps. The exposure time is set at 200 μs. The visualization on the intermediate field of view (5 cm x 7.5 cm) is performed by a Phantom V711 camera, equipped with a 70-300 mm Tamron lens, to which a focal doubling system is added. The lens aperture is fixed at f / 4. With the acquisition speed of 6000 fps chosen, a resolution of 1280x800 pixels is obtained. The camera exposure time is set at 100 μs.

Finally, for the smallest field of view (2 cm x 3.5 cm), it was necessary to use a Questar FR1MK3 lens. It is mounted on a Phantom V2512 camera, with a resolution of 1280x800 pixels with the desired acquisition rate of 18,000 fps. The exposure time of this camera is set to 40 μs. All the features of these cameras are summarized in Table 3.

Table 4: Cameras optical features

Camera	Acquisition rate	Resolution	Exposure time	Lens	Lens aperture	Field of view
V2512	18000 fps	1280x800	40 μs	Questar FR1MK3		2cm x 3.5 cm
V711	5000 fps	1280x800	100 μs	70-300 (x2)	f/4	5cm x 7.5 cm
SA3	1000 fps	1024x1024	200 μs	105 (x2)	f/2,8	10cm x 10 cm

For the tests carried out in this preliminary study, the powder mass initially inserted in each dispersion tube is 0.3 g. The pressure in the upstream tanks is set at 2.5 bar and the opening time of the solenoid valves is 0.8 seconds. This corresponds to an average dust concentration of $36 g/m3$.

2.1.3 Images obtained

Some images obtained from this preliminary study are represented in Figure 37: the three fields of view of the PIV and also the four laser beams of the LDA, corresponding to the luminous parts of the images, are distinguishable. The images relate to a fixed time (t = 0.4s after the end of the dispersion). A black circle frames the small field of view: it is characteristic of the Questar lens used.

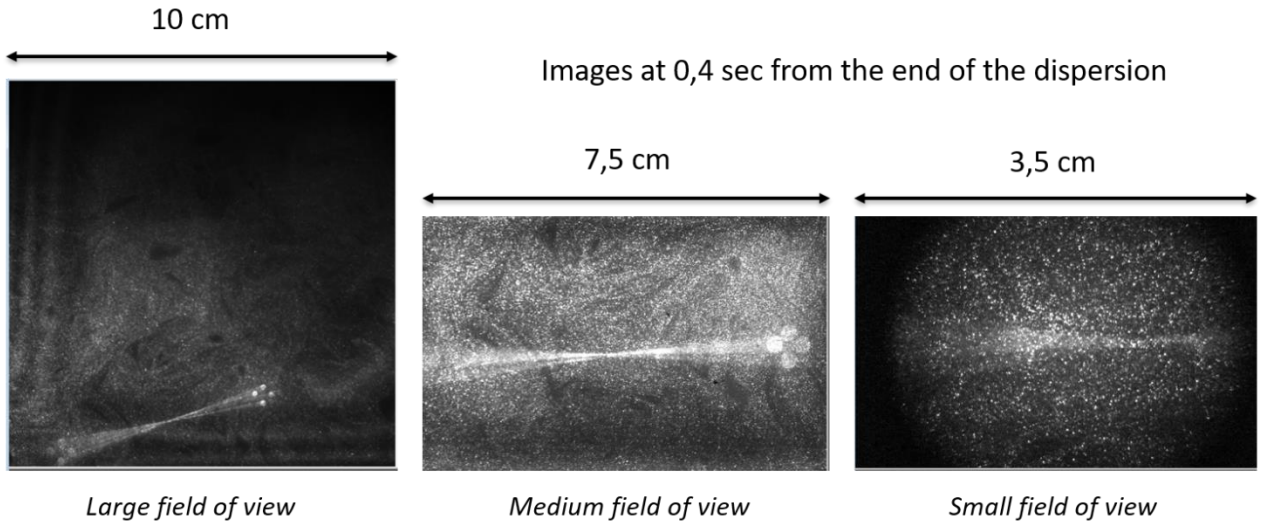

Figure 37: Images obtained for the three fields of view

2.2.4 Convergence analysis

As previously mentioned, the number of tests performed influences the turbulence results. 20 tests were realized to define the minimum number of tests allowing obtaining coherent turbulent results.

The tests number influences the calculation of the mean velocity. The first aim is to know after how many tests realized the mean velocity value stabilizes. Figure 38 shows the mean velocity calculated with a gradually increasing number of tests (for the three

fields of view). The three graphs relate to a fixed time (0.3 s after the end of the injection). Each point of the graphs is obtained as follows: an ensemble average of the velocity field has been realized between various tests; then to get a single velocity value starting from a 2D map of mean velocity (previously calculated) a spatial mean has been performed.

In the figure, the mean velocity converges to the zero value for each field of view. In the case of the small field, a lower number of tests is needed to reach the convergence of mean velocity.

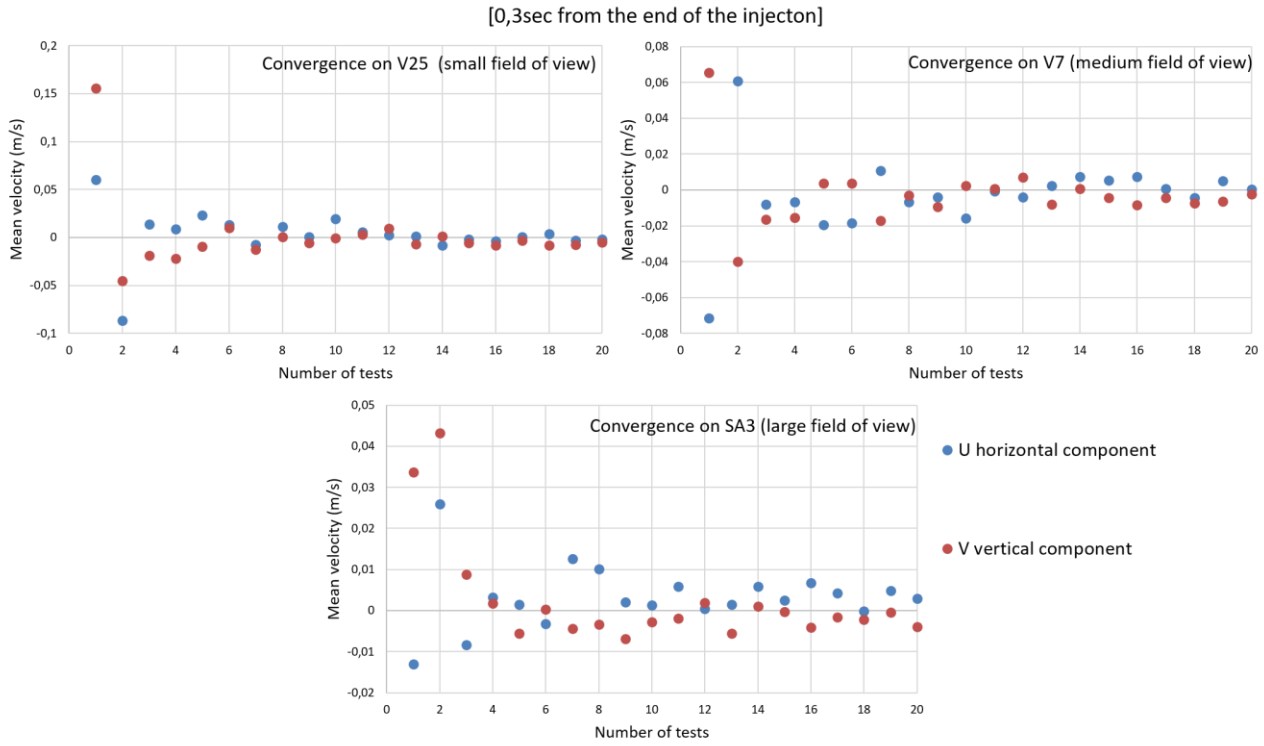

Figure 38: Convergence of mean velocity over the number of tests

From this mean velocity, the intensity of turbulence can be calculated. The aim of this

part of this study is to define the minimum number of tests starting from which the value of turbulence intensity stabilizes: this means that an increase in the number of tests used to calculate turbulence intensity will change weakly the value registered. Figure 39 shows the evolution of the turbulence intensity calculated by modifying the number of tests used. These results correspond to the intermediate field of view. The different curves correspond to the results obtained at different times after the end of the injection. First, turbulence intensity decreases with time after the end of the injection. Furthermore, convergence of turbulence intensity is observed for each time step after about 8 tests performed; in other turbulence measurement tests at least 8 tests should be performed.

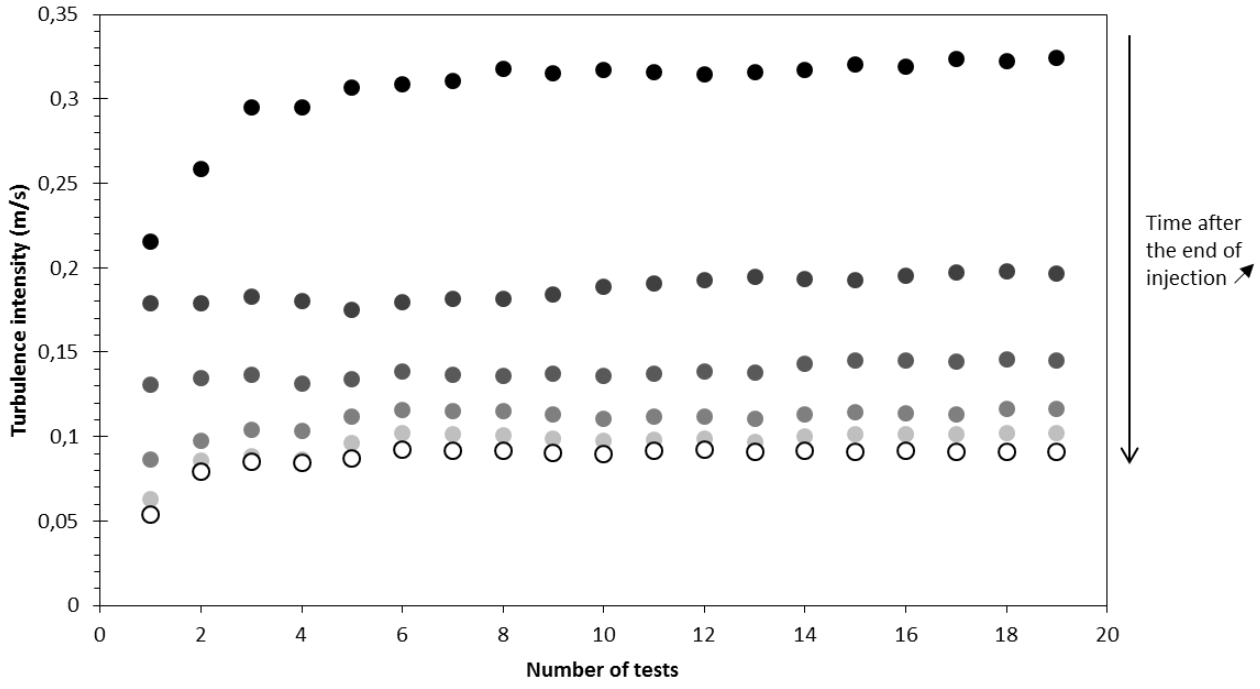

Figure 39: Convergence of turbulence intensity over time and on the number of tests performed (time between each curve: 200 ms)

2.2.5 Determination of the field of view for PIV measurements

Based on the results obtained for the 20 tests, the evolution of turbulence intensity over time for each field of view can be compared. Figure 40 shows the turbulence intensity colormaps obtained for each fields of view, for three different times (0.2s, 0.6s, and 1s after the end of the injection).

The red areas on the images, obtained for the small field of view, correspond to the dark circle due to the QUESTAR lens. The areas in blue, particularly visible in the intermediate and large field images, correspond to the LDA laser beams.

The turbulence level appears to be globally spatially homogeneous for each field of view from 0.6 seconds after the end of the injection.

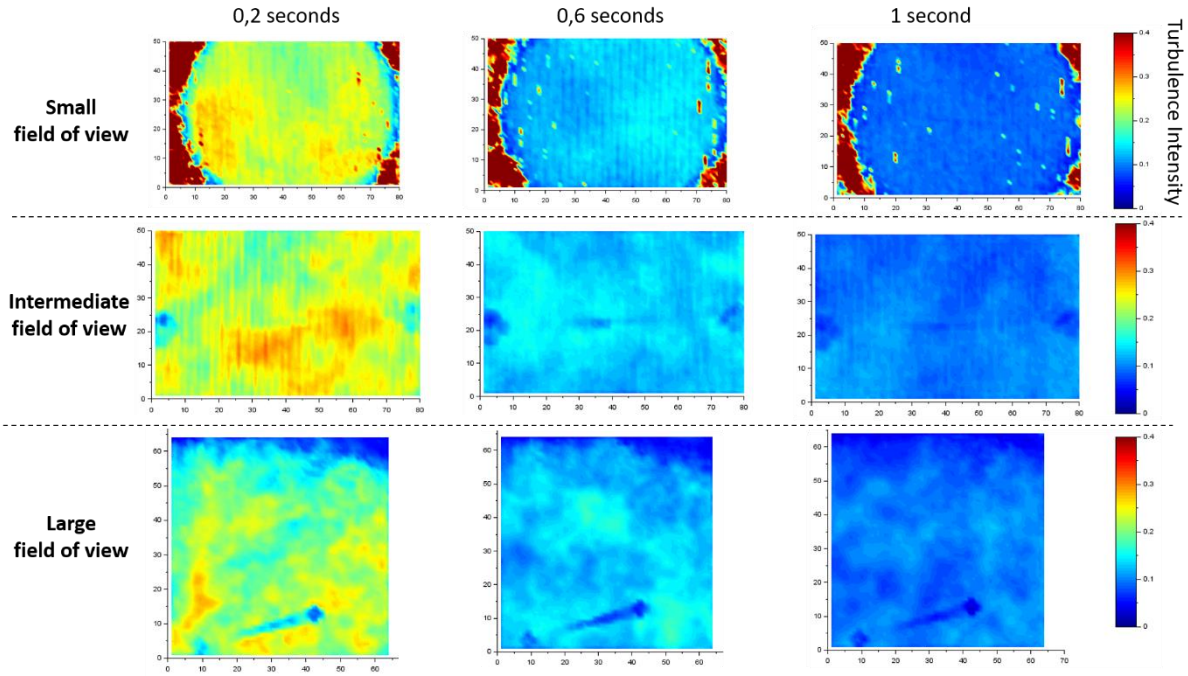

Figure 40: Colormaps of turbulence intensity for the three fields of vies and their evolution overtime

A decrease in the turbulence level is observed for each field of view after the end of the injection. To quantify this decrease in turbulence, the spatial mean has been calculated from all interrogation areas of the maps. The evolutions of these mean turbulence

intensities are shown in Figure 41 for each field of view. A difference in the mean turbulence intensity calculated for each field of view studied is observed. The smaller the field of view, the more the mean turbulence level seems important. The large field of view allows the quantification of turbulence associated only with vortices larger than those that can be detected by the other two cameras. Therefore, it seems consistent to achieve a higher level of turbulence with smaller fields of view.

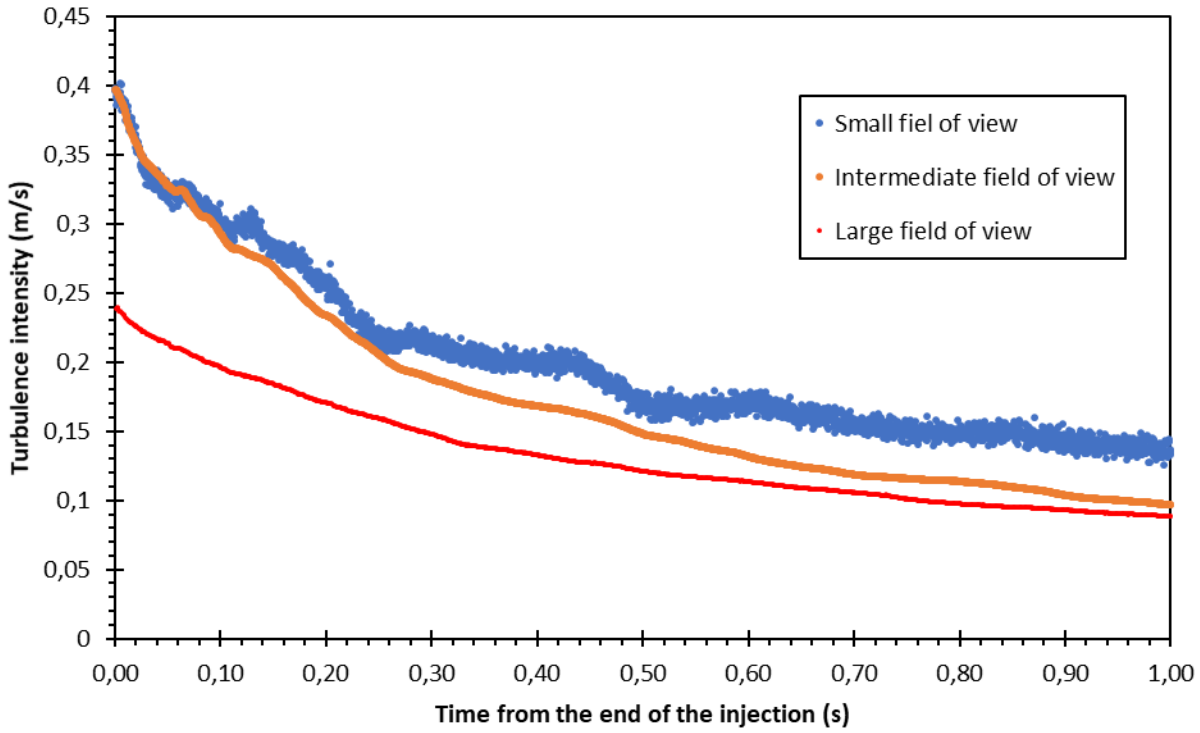

Figure 41: Turbulence intensity evolution overtime, spatial mean on each field of view

In Figure 41, the spatial average of the turbulence level is shown. But this average is performed on physical areas of different sizes: the area used for calculating the spatial average is greater for the larger field than that used for the small field.

A new spatial average has been studied, considering the same physical areas for each

field of view. Thus, the only difference between the fields of view lies in the difference in spatial resolution of the studied interrogation areas. It is important to note that to get the same physical measurement zones, the number of interrogation areas used for each field of view is different: the number of interrogation areas becomes higher passing from the large field of view to the small one.

Figure 42 shows the evolution of mean turbulence intensity, where its spatial mean is calculated on the same physical area for each field of view. The decay of turbulence level over time (after the end of the injection) is observed for each field of view. Furthermore, the turbulence levels measured inside the small and intermediate field of view are close. The large field of view generally underestimates the turbulence level within the flow. From $t = 0.7s$ after the end of the injection, the turbulence data obtained with each field of view are close; turbulence intensity value is around 0.1 m / s.

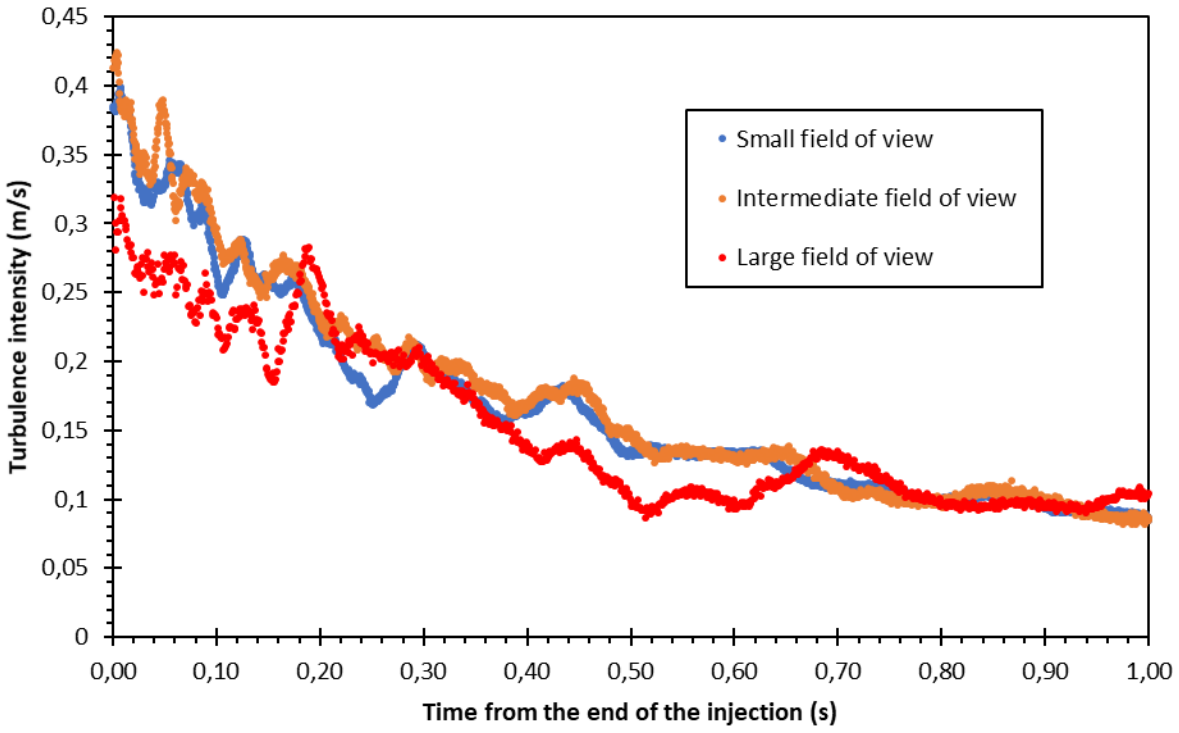

Figure 42: Turbulence intensity overtime, mean on physical space

2.2.6 Comparison with the LDA measure

Turbulence data measured by LDA can be compared with those obtained by the different scales of PIV. The analysis method of LDA data to quantify turbulence is specified in Chapter 2. To calculate velocity fluctuations a mean velocity equal to zero is considered. This zero value is consistent with the results obtained by PIV as exposed in Figure 38.

Figure 43 shows again the evolution of the turbulence intensity for each field of view, with a spatial mean corresponding to the same physical area. On this graph, the LDA results are added. The data obtained with the LDA are in good agreement with the results previously presented: the same decrease in turbulence over time is observed. The PIV data obtained in the small field of view are about 20% lower than those obtained by LDA. Measurements by LDA are local, with a high acquisition frequency, thus allowing access to the turbulence contained in a larger range of vortices. This explains a higher calculated turbulence intensity in the case of LDA measurement. Apparently, the most reliable value of turbulence intensity by PIV is obtained with the small field: it accesses to the energy contained in the vortices of smaller dimensions.

This difference in turbulence intensity level can also be explained by the different analysis method followed in the two types of measurements. Indeed, in the case of the PIV, an ensemble average on all the tests is carried out in order to obtain the turbulence data. On the contrary, in the case of the LDA, the fluctuations are averaged by time intervals: an ensemble average is subsequently used to take into account the turbulence of the different tests performed.

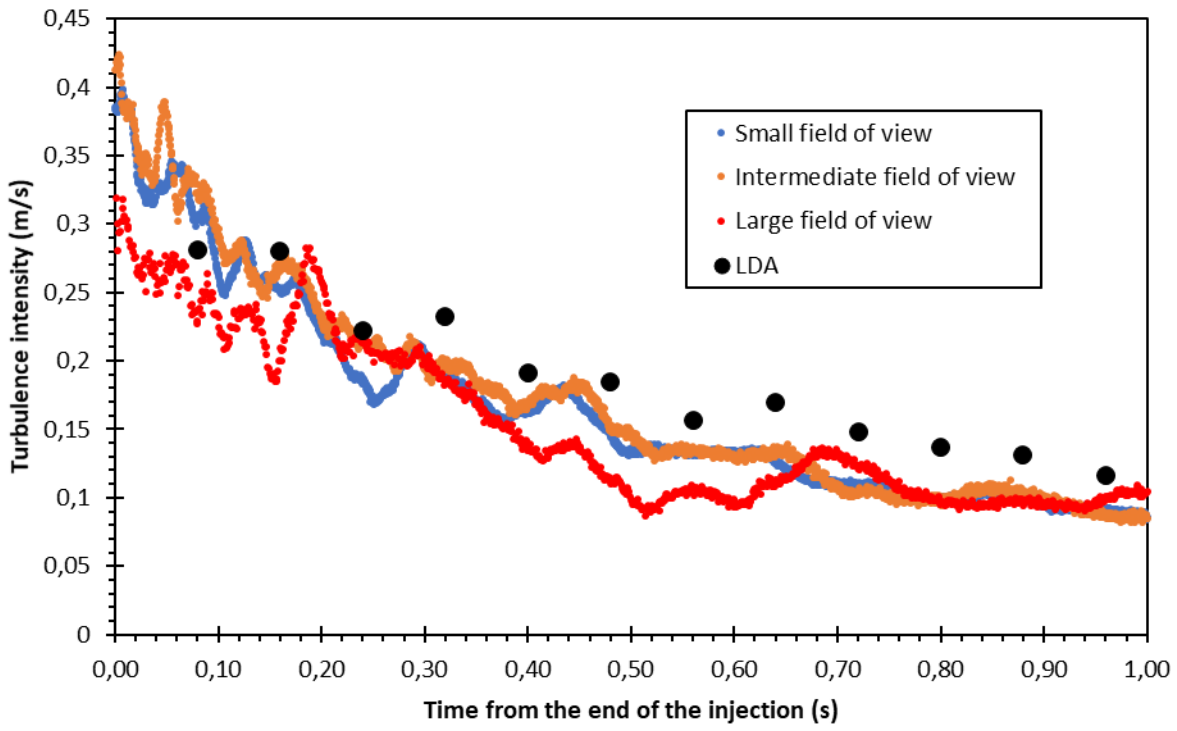

Figure 43: Turbulence intensity overtime, comparison between PIV and LDA data

2.2.7 Conclusions

This preliminary study investigated the influence of the size of the field of view chosen to perform PIV on the turbulence level results. Three high speed cameras have been used to visualize the flow by PIV, with three measurement areas of different sizes. A measurement by LDA, in the area common to the three previous PIV measurements, was also performed.

The turbulence data obtained with the small and the intermediate fields of view are fairly close. The data obtained with the large field of view are weaker; this field of view accesses only to the energy contained in the larger vortices.

The LDA and PIV results have been compared, and the same turbulence decay behavior has been observed. The data with the PIV small field of view are smaller than those obtained by LDA by about 20%.

This study gives us information which will be useful in the subsequent turbulence studies. In the following PIV measurements, a field of view of the order of magnitude of the intermediate field of view studied here will be chosen: 5cm x 7.5cm. Indeed, the data obtained with the small field are fairly close to those obtained with the intermediate field. The intermediate field is thus a compromise in terms of the result obtained and the quality of the images (black circles around the images obtained with the QUESTAR lens).

The study of the convergence of the turbulence data as a function of the number of tests was carried out on 20 tests. The turbulence intensity varies only slightly beyond about eight tests carried out. Thus, in the following studies, the PIV turbulence data will be obtained from at least eight tests.

2.2 Analysis of dispersion-induced turbulence decay

In this part, the evolution of turbulence intensity after the end of particle injection has been analyzed. Two dust dispersion configurations have been studied, defined by the initial pressure in the air tanks and the injection time. As for Mie scattering tests, the first configuration corresponds to an initial pressure of 2.5 bar and to an injection time of 800 ms; the second corresponds to a pressure of 4 bar and an injection time of 300 ms.

2.2.1 Presentation of the tests

The turbulence level of the suspension obtained in two dispersion configurations (4b / 300ms and 2.5b / 800ms) is measured with the PIV and LDA techniques. The initial mass introduced is equal to 0.3g in each injection tube. Indeed, a low mass of dust is mandatory for these techniques.

PIV measurements were performed using a LITRON pulsed laser (200 mJ at 15 Hz) equipped with a laser sheet generator. The delay between the laser pulses is fixed at

300μs. The camera used is a HAMAMATSU HiSense camera with a resolution of 2048x2048 pixels at the chosen acquisition frequency of 10 Hz. The time between two pairs of images (corresponding to two velocity maps after digital processing) is 200 ms. The camera is equipped with a Nikkor lens with a fixed focal length of 105 mm, combined with a focal doubling system. The aperture of this lens is set to f / 4. The PIV measurement area is 4.9 cm x 4.9 cm, in line with the results of the study on the influence of the measurement area on PIV results. 10 tests were performed for each dispersion configurations; again in accordance with the previous preliminary study.

2.2.2. Results

The images obtained in the PIV tests were analyzed using the DynamicStudio software, which returns 2D maps of instantaneous velocity for each pair of images of each test. At each instant, an ensemble average between the velocity maps of the various tests has been calculated. A single sequence of average velocity fields is thus obtained.

At each instant, for each velocity field, a spatial average is made to obtain a single mean value of the velocity: to do that, an average is performed between the velocity values of each interrogation area.

In the end, the graph represented in Figure 44 is obtained: the values of the horizontal ($\bar{u}$) and vertical ($\bar{v}$) components of the mean velocity over time are shown.

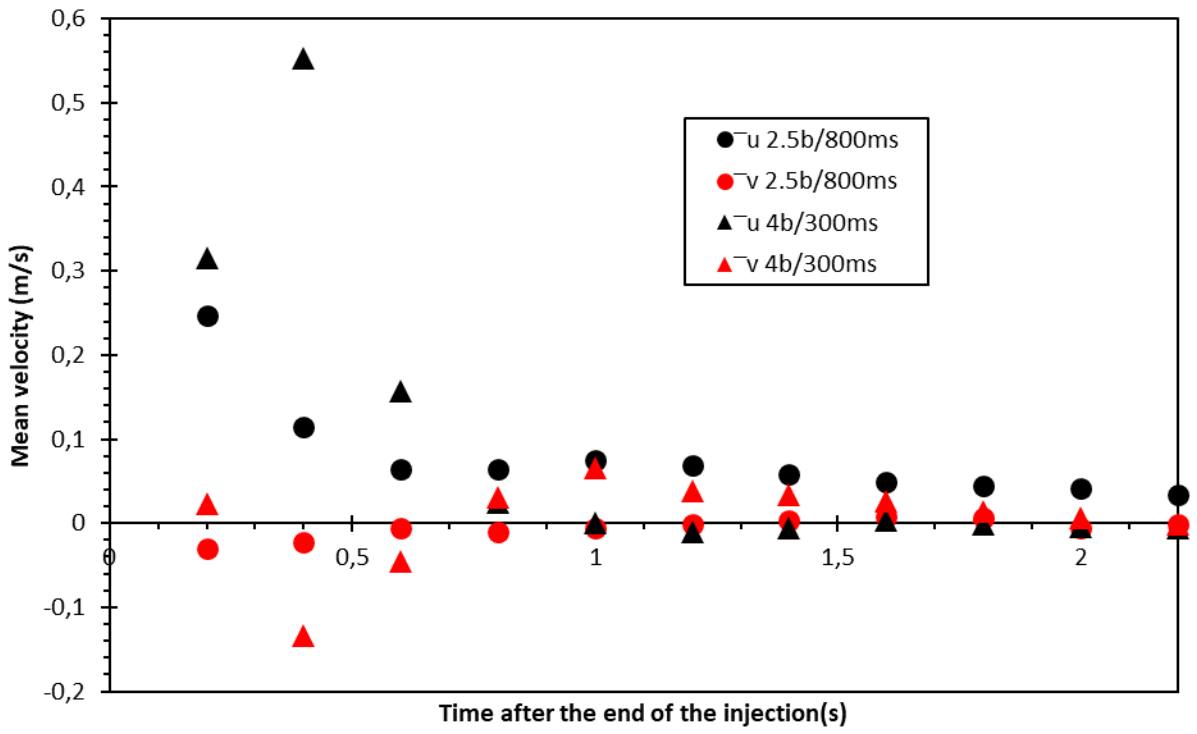

Figure 44: Evolution of average velocity components over time for both dust dispersion configurations

The average velocity decreases until a zero value. Therefore, no general preferential movement seems to be present within the flow.

In the case of a 4b / 300ms injection, the mean velocity is globally higher than for the other configuration. In fact, in the case of such a fast injection, the jet effect that introduces the dust into the flow is still present when the solenoid valves are closed. On the contrary, in the case of an injection at 2.5 b / 800 ms, when the solenoid valves are closed this jet effect is very attenuated; the pressure in the upstream tanks being close to the atmospheric pressure.

From these mean velocity values, the fluctuating components of the speed are obtained. The trends of u' and v' over time are shown in the semilogarithmic graph presented in Figure 45.

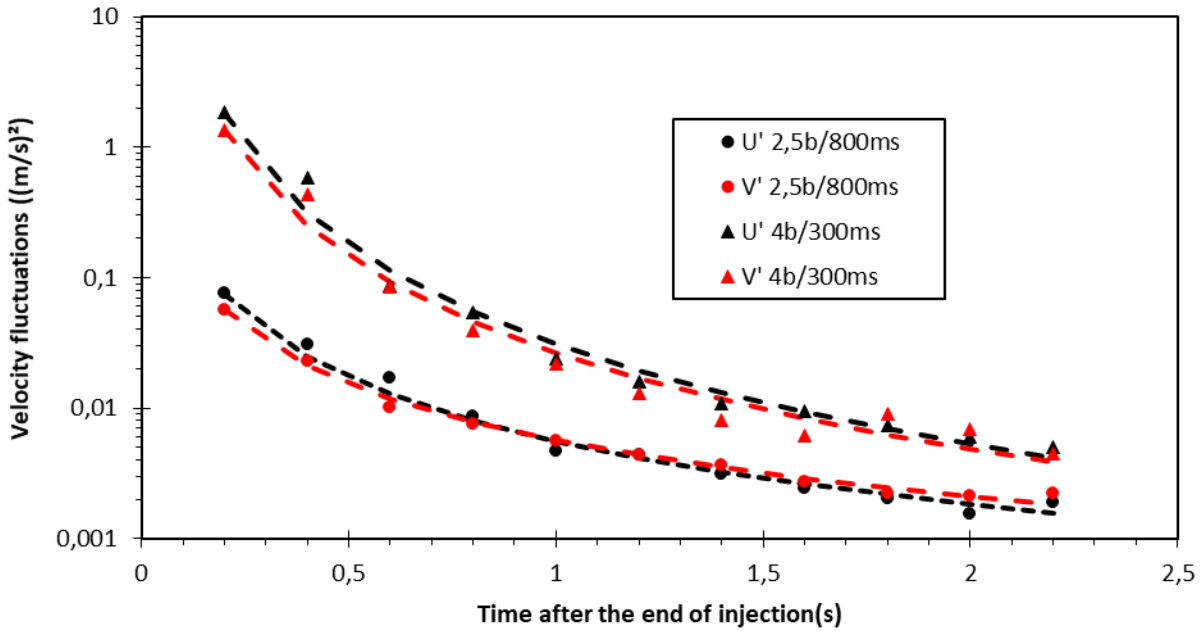

Figure 45: Evolution of fluctuating velocity components over time for both dust dispersion configurations

The fluctuation speeds obtained with the 4b / 300ms injection are greater than those obtained with the 2.5b / 800ms configuration. As previously mentioned, the quantity of air introduced in the two configurations is the same. However, with the first configuration, the air is injected faster (300 ms) than the second (800 ms). The flow is, therefore, more turbulent in the 4b / 300ms configuration and will require a longer time to relax. Furthermore, for both the configurations studied, the horizontal (u') and vertical (v') fluctuations are close.

The intensity of the turbulence is then determined for each of the two experimental configurations. Its decay is shown in Figure 46.

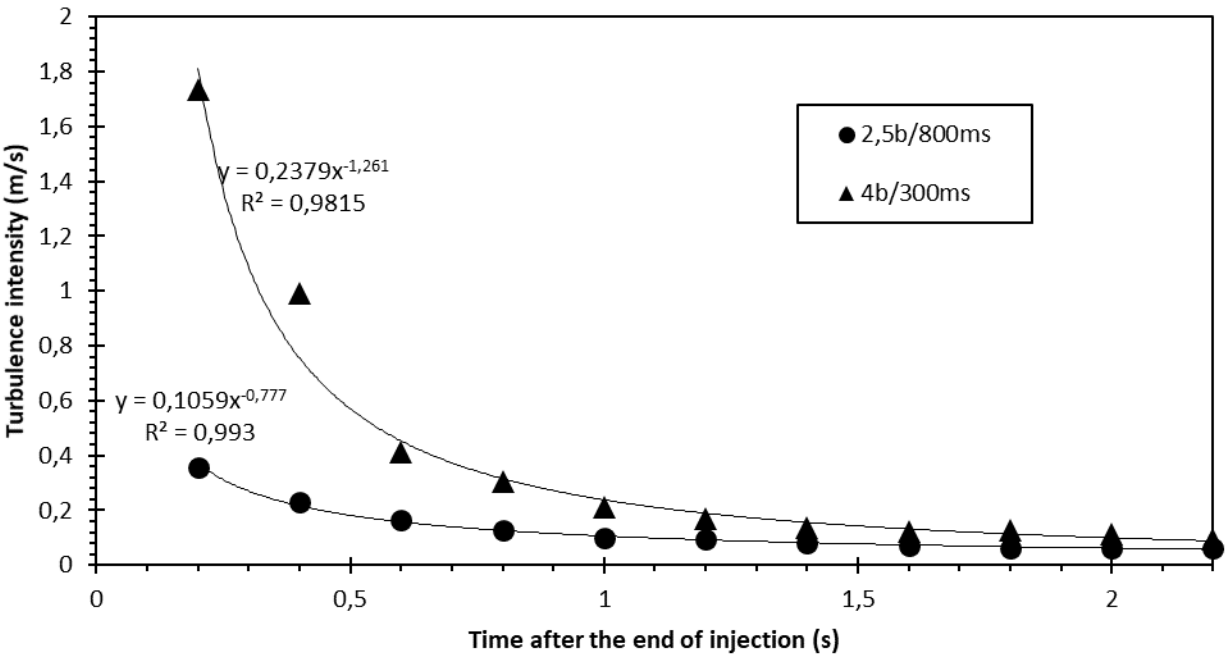

Figure 46: Evolution of turbulence intensity over time for both dust dispersion configurations

The turbulence intensity is higher with 4b / 300ms injection, as already noted. Although the turbulence intensity obtained with the 4b / 300ms configuration is higher, the latter decreases more rapidly than the one obtained at 2.5b / 800ms. The turbulence intensity is 1.73m/s, 200ms after the end of the injection, in the 4b / 300ms configuration and decreases to a value of 0.11m/s after a delay of 2s after the end of the injection. In the 2.5b / 800ms configuration, for the same delays after the end of the injection, the turbulence intensity, initially of 0.36 m/s, decreases only up to a value of 0.06 m/s.

During the previous tests, LDA measurements were also carried out. The two methods are indeed complementary. It is interesting to analyze the comparison between the data obtained with these two measurement techniques.

The LDA allows obtaining the temporal variations of two components of the flow velocity in a point of the flow: u is the horizontal component and v is the vertical

component. Following the method presented in Chapter 2, it was possible to switch from the values of the instantaneous velocity measured in the tests to the trend of the fluctuating components of the velocity for both experimental configurations (2.5bar / 800ms) and (4bar / 300ms). From the fluctuating components the turbulence intensity in the two dispersion configurations is calculated. The Figure 47 shows the comparison between the PIV results and the LDA results related to the evolution of turbulence intensity for both injection configurations.

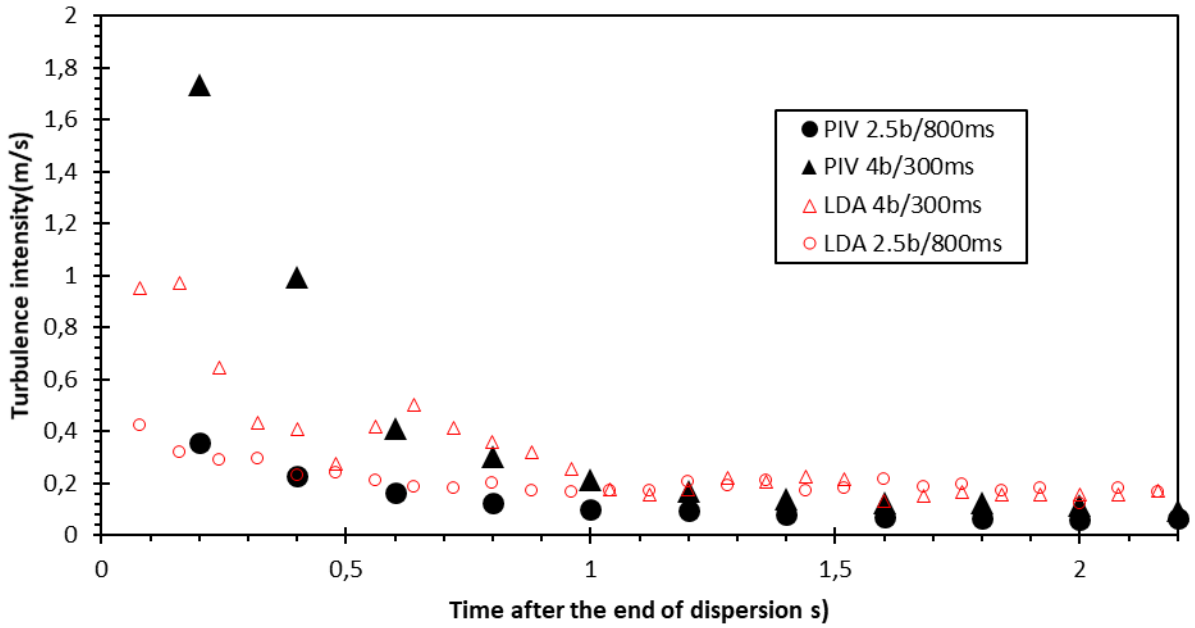

Figure 47: Turbulence intensity over time . Comparison between PIV and LDA results for both dust dispersion configurations

The results of PIV and LDA present a similar trend in the 2.5bar / 800ms dispersion configuration.

In the 4bar / 300ms configuration, the turbulence trend is similar for the two methods only starting from 600 ms after the end of the suspension injection; for times shorter than 600ms the PIV registers turbulence levels higher than those recorded by the LDA. This difference in the data is due to the criterion chosen for the LDA measurements: the range of measurable velocities is set at about +/- 1.2m/s. Thus particles having a velocity

outside this range are not validated. In this case, LDA underestimates instantaneous velocity and therefore turbulence intensity. The enlargement of the identifiable velocity range led to the appearance of a significant noise during the measurement. The noise increases as we move away from the time of the end of the injection. Therefore it was preferred to maintain the range +/- 1.2m/s. In fact, the level of turbulence when the mixture is ignited has to be investigated. From the concentration study, we concluded that this ignition will not take place immediately after the injection, as the homogeneity of the suspension is low. For this reason, the turbulence data just after the end of injection are less important for this study than those obtained for a longer period.

2.2.3 Conclusions

Tests to determine the turbulence level of the aluminum powder suspension have been carried out. The methods of investigation were the PIV and the LDA. Two dispersion configurations were analyzed: 2.5 bar / 800ms and 4bar / 300ms. In the first configuration, the level of turbulence recorded is not very high, but its decay is slower. In the second configuration, immediately after the end of the powder injection, a higher level of turbulence is recorded, but it decays almost immediately.

The dust-air suspension of dust has been characterized both in terms of concentration and turbulence; the flame propagation can now be investigated.

3. Influence of dispersion-turbulence on flame propagation

In this part, the study on flame propagation is carried out: the propagation happens in the same prototype used to study dispersion. However, it is equipped with the trigger system described in Chapter 2. Two electrodes were placed at the base of the prototype to allow the ignition of the mixture.

The study of the flame behavior is based on two elements: the overpressure generated by the deflagration (recorded by pressure sensors) and the flame propagation velocity (recorded by a high speed camera). In all this part, only the pressure data corresponding to the upper pressure sensor are exposed. As previously mentioned, the data from both pressure sensors are fairly, but the upper sensor is more sensitive.

First, an example of one flame propagation test and the corresponding anaylsis are exposed. At the end of this part the influence of dispersion-induced turbulence on flame propagation is investigated. In order to obtain different levels of turbulence within the suspension, different delay times are chosen between the end of the injection and the moment of ignition.

3.1 Visualization of aluminum dust flame propagation during one test

3.1.1 Test presentation

As already mentioned, a propagation test is performed as follows: the powder is weighed and loaded into the injection tubes. The air tanks are brought to the desired pressure. The solenoid valves are opened and the air is discharged: the suspension enters the prototype. The moment in which the valves close corresponds to the end of the injection. After waiting for a so-called dead time t_{delay} (modifiable) the trigger occurs. The duration of the electric arc (t_{arc}) can be changed. At the end of the test, by weighting the dust remained in the tubes, the concentration of the suspension is

calculated.

Numerous flame propagation tests have been carried out in two different dispersion configurations: 2.5bar / 800ms and 4bar / 300ms. The test presented hereafter corresponds to the dispersion configuration 4b / 300 ms. The dust mass inserted in each injection tube is 2.8 g. The corresponding concentration measured is around 480 g/m^3. For this test, the time between the end of the injection and the ignition of the dust cloud is chosen to be 1 s. The characteristics of the pressure sensors and of the high speed camera have already been detailed in Chapter 2.

3.1.2 Phenomenon of flame propagation

Figure 48 shows the evolution of pressure during the propagation test. The red vertical lines correspond to specific instants of the flame propagation phenomenon. The images, recorded by the high speed camera, corresponding to the instants of the red lines are exposed on Figure 49.

During the propagation of the flame front inside the visualization part of the prototype, non-saturated images are obtained. If some parts appear saturated, this is due to a numerical treatment of the raw images for display purpose.

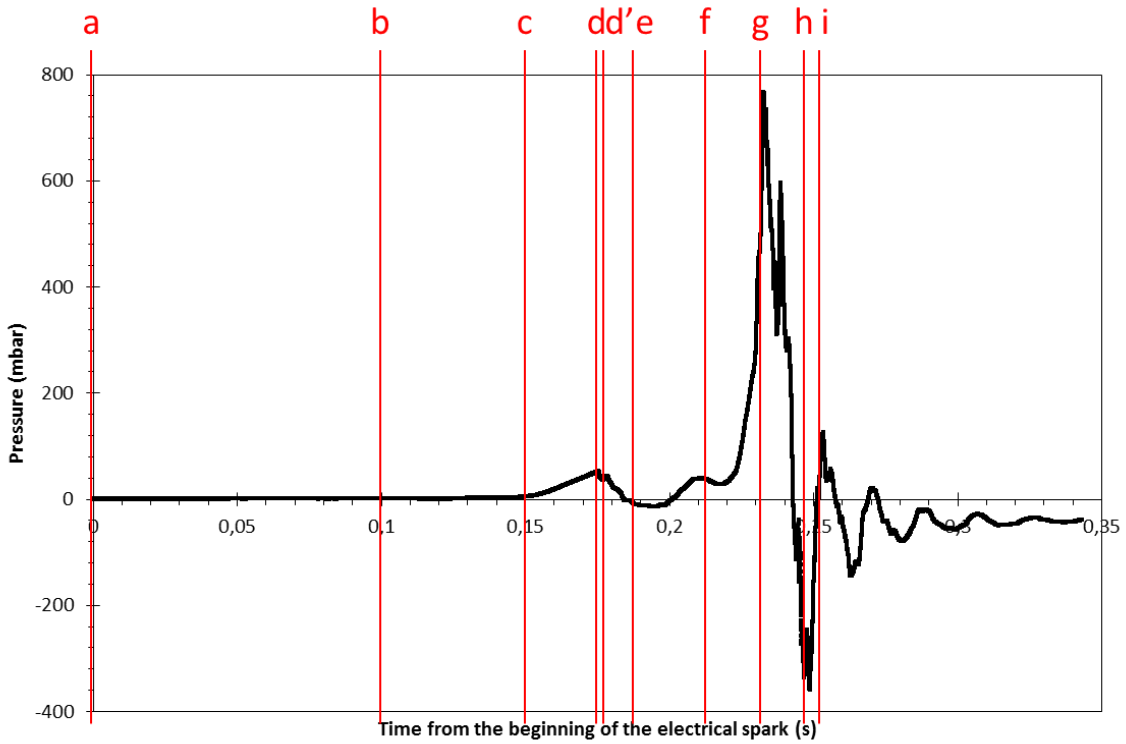

Figure 48: Pressure evolution during flame propagation

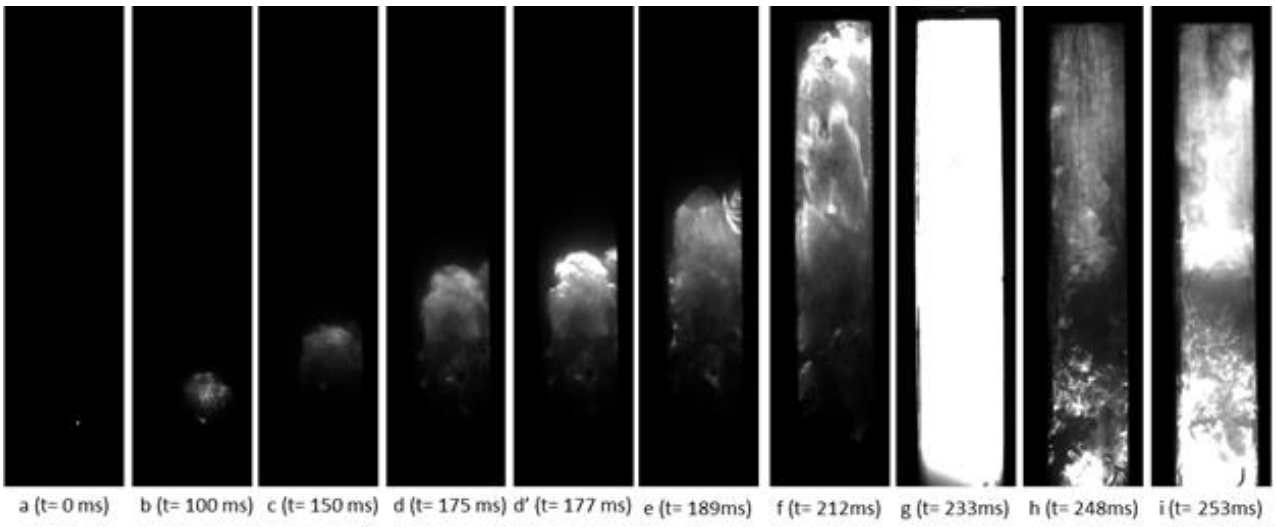

Figure 49: Flame propagation visualization

The flame propagation phenomenon is explained hereafter thanks to the two previous

figures.

At the instant t = 0 ms (a), the dust has already been dispersed inside the vessel, and the spark is turned on. At this instant, the pressure inside the prototype is the atmospheric pressure. Indeed, the introduction of the suspension inside the prototype causes a change in the confinement volume: the membrane "swells" up to a certain point. By this way, the membrane keeps the atmospheric pressure inside the vessel.

At the instant t = 100 ms (b), the spark is stopped. At this moment a flame detached from the initial spark is distinguishable.

At the instant t = 150 ms (c), an increase of the pressure is observed. At this moment, the membrane has reached its maximum extension. Indeed, when the suspension is ignited and the flame propagates, the membrane extends further, and the pressure in the confinement is maintained at his atmospheric value. When the membrane can no longer swell, the confinement volume remains fixed, and the flame propagation generates an increase in pressure inside the prototype.

At the instant t = 175 ms (d), the pressure starts to decrease; this moment corresponds to the rupture of the membrane. The membrane has been chosen for its low resistance to pressure increase to avoid disturbing the flame propagation: in particular, the rupture occurs at around 35 mbar of overpressure. Just after the rupture of the disk, at the instant t = 177 ms (d'), there is a small surge in pressure: in the images this corresponds to a moment in which the flame front becomes more luminous.

Then the pressure drops to negative values; in the images at the instant t = 189 ms (e) small flames which coming out from the injection tubes are distinguishable.

The flame leaves the visualization part at the instant t = 210 ms (f); there is a local maximum in the pressure graph corresponding to this moment.

At the instant t = 220 ms (g) a pressure peak is observed in the pressure graph. The flame front is out of the visualization part and is propagating through the exhaust duct at the top of the prototype. In the visualization part, the flame appears extremely bright

at this time. After this peak the pressure begins to decrease, going down to negative values; the flame decreases its brightness. Subsequently, oscillations are observed, both in the pressure values and in the luminous intensity.

3.1.3 Results analysis

From the images experimentally obtained, the course of the flame front can be analyzed. In the graph of Figure 50, the evolution of the position reached by the highest point of the flame font in its propagation is represented by the black curve. The last plotted position corresponds to the moment in which the flame front leaves the visualization part. The evolution of the flame front position over time (black curve) seems to follow a second-order polynomial. This corresponds to a flame propagation with a constant velocity. The best second-order polynomial fitting this curve is represented by the orange curve. However, the direct calculation of the flame speed by direct derivative of the position curve shows a more complex trend (red curve); the evolution of this velocity presents some fluctuations during its propagation.

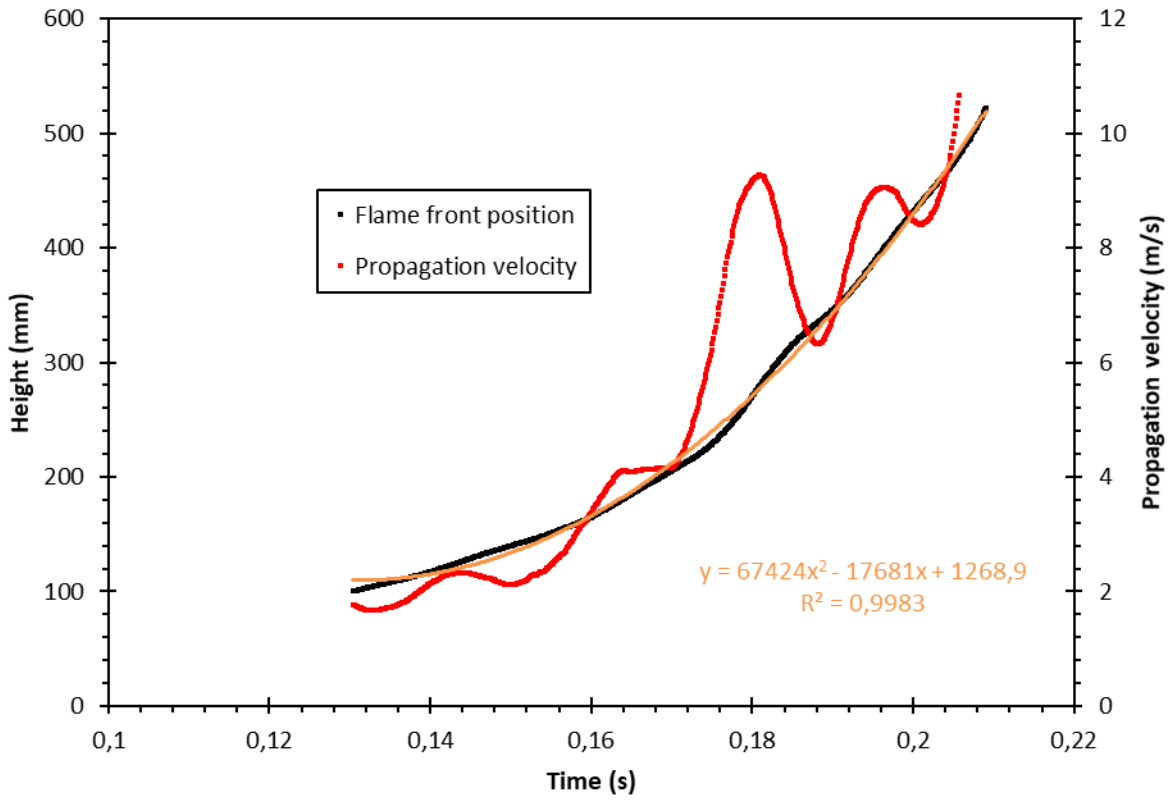

Figure 50: Flame front position and velocity

Propagation velocity (red curve) is exposed again in Figure 51. In the same figure, the pressure (green curve) and light intensity (orange curve) evolutions are also represented. The light intensity trend is obtained considering a spatial mean on the grey levels of each image.

The evolutions of these three variables are fairly close. The higher value of pressure corresponds to a peak in terms of velocity and light intensity as well. The fluctuating behavior of velocity also appears in the pressure and light intensity curves. Fluctuations of light intensity and pressure continue to be linked even after the flame leaves the visualization part. This pulsating behavior, especially in terms of light intensity, has already been observed during aluminium flame propagation (Julien et al. 2015).

For studying and comparing results of flame propagation, three parameters are defined: the maximum overpressure (P_{max}), the maximum of pressure rise ($(dP/dt)_{max}$) and the

maximum flame velocity (V_{max}). These three parameters are defined only while the flame front propagates inside the visualization part.

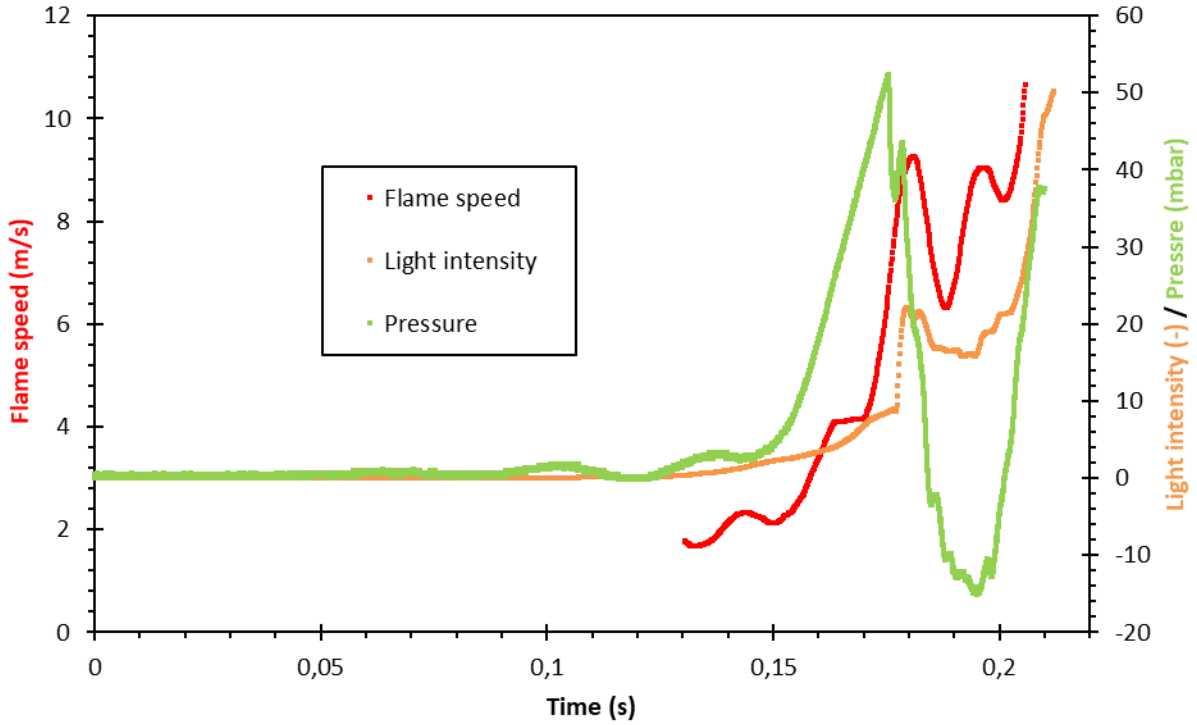

Figure 51: Propagation velocity, pressure, light intensity over time

3.2 Study of the influence of dispersion-induced turbulence

In this part, the influence of dispersion-induced turbulence at the moment of ignition on flame propagation parameters is investigated.

This study is based on the results of parts 1 and 2 of this chapter. The results of these parts showed that between the two dispersion configurations analyzed (4bar / 300ms and 2.5bar / 800ms), the highest turbulence levels are reached in the configuration corresponding to a pressure in the air tanks equals to 4bar and an injection time of 300 ms. This configuration is therefore used to analyze the influence of turbulence on propagation parameters.

As previously mentioned, the ignition should happen when the suspension is

sufficiently homogeneous (+/- 20%). The minimum delay to respect this criterion is 600 ms.

It has been demonstrated experimentally that homogeneity and turbulence have opposite trends over time. Therefore the choice of the ignition moment represents a compromise between the level of homogeneity and turbulence. The propagation tests were performed using two trigger times: 600 ms and 1 s. The delay of 600 ms corresponds to the maximum of turbulence when the suspension is homogeneous. For this delay, the turbulence intensity is equal to 41cm / s. With the delay of 1s the turbulence intensity drops to 21cm / s.

Using the dispersion configuration corresponding to 4bar / 300ms, six tests were carried out with a delay (between the end of the dispersion and the ignition) of 600ms and five tests with a delay of 1s. These tests were analyzed to extract the three previous parameters for each test. Table 5 shows the results of each test.

Table 5: Summary of parameters obtained for each test

Delay before ignition (s)	Test	Pmax (mbar)	(dP/dt)max (bar/s)	Vmax (m/s)
1	1	31.2	4.0	13.9
	2	32.0	3.6	9.0
	3	40.5	5.4	13.8
	4	33.0	4.8	12.6
	5	47.4	5.5	10.7
0.6	1	24.2	3.2	14.0
	2	45.1	5.5	13.9
	3	37.6	3.6	11.2
	4	44.4	3.6	8.8
	5	47.4	4.8	11.4
	6	34.3	4.3	11.4

For the two configurations, the mean and the standard deviation of each parameter, based on the different tests realized, have been calculated. These data are summarized in Table 6. The results show that no general influence of the initial turbulence intensity on these flame propagation parameters is observed, according to the repeatability of the tests. This absence of influence is probably due to low levels of initial turbulence. Indeed, the two initial levels of turbulence investigated are quite close and in both case turbulence intensity is not very high. These turbulence levels were chosen to obtain a relatively homogeneous suspension at the time of ignition, corresponding to low level of turbulence. In this case, propagation is mainly influenced by the generation of turbulence at the walls rather than by the initial turbulence.

Other injection systems could be investigated, in order to obtain a homogeneous mixture in terms of concentration with higher levels of initial turbulence. With this current dispersion system, influence of turbulence on flame propagation could be analyzed thanks to obstacles positioned along the height of the prototype.

Table 6: Influence of turbulence intenisty on flame propagation parameters

	0.6 sec time delay (IT=41cm/s)			**1 sec time delay (IT=21cm/s)**		
Parameter analyzed	Mean on the tests	Standard deviation	Ratio	Mean on the tests	Standard deviation	Ratio
Pmax (mbar)	38.8	8.7	22%	36.8	7	19%
dP/dt max (bar/s)	4.1	0.8	20%	4.6	0.8	18%
Vmax (m/s)	13.5	4.3	32%	12	2.1	18%

Conclusions

This thesis consisted of an experimental study of dust dispersion characterization and its influence on flame propagation. The aim was to investigate the link between dispersion-induced turbulence on the parameters of the explosion. The dust chosen for this study is aluminum, a metallic dangerous substance which finds uses in several industries.

After a first literature review on the phenomenon, the methods used for this study are illustrated. The experimental work carried out in the laboratory, and its results were also described.

Mie scattering was performed to measure the concentration level within the suspension. The homogeneity level of the suspension and its evolution over time were measured. A delay of around 600 ms after the end of the dust injection was prescribed to obtain a globally homogeneous suspension (criterion: +/- 20%).

PIV and LDA were used to measure the decay of turbulence level. The conditions under which the PIV was performed were chosen based on the results of a preliminary analysis. The preliminary analysis aimed to find the best field of view for the PIV measurement (around 5 cm x 7.5 cm). Moreover, a converge analysis of the recorded turbulence intensity values has been carried out: the minimum number of tests necessary to get reliable results from a statistical point of view has thus been defined (at least 8 tests).

The PIV and the LDA allowed obtaining the evolution of turbulence intensity over time. This data was important to quantify the turbulence level at the moment of ignition. Moreover, modifying the delay between the end of the injection and the ignition, the turbulence intensity level is modified.

The study of dispersion in terms of homogeneity and turbulence led to the following conclusions: immediately after the end of the injection of the dust, the suspension is turbulent and not very homogeneous. There are strong concentration gradients within the flow. Over time the turbulence decreases and the level of homogeneity increases.

Flame propagation tests have been performed. In each test, it was possible to measure the main parameters (maximum overpressure and maximum pressure rise velocity) using pressure sensors, and the maximum flame propagation velocity by processing the data obtained by direct visualization of the flame front.
The ignition times of the suspension have been chosen in order to have different levels of initial turbulence within the suspension. In this way, the influence of turbulence on flame propagation is analyzed. The two levels of turbulence intensity investigated are 21 cm/s and 41 cm/s. With these two levels, no influence of dispersion-induced turbulence on flame propagation can be drawn, according to the repeatability of the tests. Indeed, these two levels are too weak and too close. It was not possible to carry out propagation tests at very high turbulence levels since the suspension must be homogeneous at the time of ignition; flow homogeneity corresponding to weak turbulence levels.

For future experiments, new dispersion systems could be tested, which would allow obtaining a homogeneous suspension, simultaneously characterized by a higher turbulence level. With this dispersion system, influence on turbulence on flame propagation could be investigated adding obstacles positioned along the height of this prototype.

References

Amyotte, P., 2013. An Introduction to Dust Explosions: Understanding the Myths and Realities of Dust Explosions for a Safer Workplace, An Introduction to Dust Explosions: Understanding the Myths and Realities of Dust Explosions for a Safer Workplace. doi:10.1016/C2011-0-07244-7

Bartknecht, W., 1989. Dust-explosions: course, prevention, protection, Journal of Loss Prevention in the Process Industries. doi:10.1016/S0950-4230(97)00026-0

Berg, A.E., Christiansen, M.G., Balakin, B. V., Kosinski, P., 2018. Investigation of dust dispersion in a modified Hartmann tube using positron emission particle tracking and simulations. J. Loss Prev. Process Ind. 55, 178–190. doi:10.1016/j.jlp.2018.06.007

Bozier, O., 2004. Contribution à l'étude des caractéristiques de combustion isochore d'une suspension de particules solides réactives. Génération d ela suspension; influence de l'état initial du mélange.

Chanut, C., 2018. Etude expérimentale de la propagation du front de flamme et de la vitesse de combustion d ' une explosion de poussières d ' aluminium.

Chanut, C., Heymes, F., Lauret, P., Slangen, P., 2018. Visualization of aluminum dust flame propagation in a square-section tube. Chem. Eng. Trans. 67, 7–12. doi:10.3303/CET1867002

Cuervo, N., 2015. Influences of turbulence and combustion regimes on explosions of gas-dust hydrid mixtures.

Dahoe, A.E., 2000. Dust explosions: a Study of Flame Propagation.

Dahoe, A.E., Cant, R.S., Scarlett, B., 2001. On the transient flow in the 20-liter explosion sphere. Flow, Turbul. Combust. 14, 159–184. doi:10.1023/A:1015099110942

Eckhoff, R.K., 2003. Dust Explosion in the Process Industries, Online.

Galmiche, B., Mazellier, N., Halter, F., Foucher, F., 2014. Turbulence characterization of a high-pressure high-temperature fan-stirred combustion vessel using LDV, PIV and TR-PIV measurements. Exp. Fluids 55. doi:10.1007/s00348-013-1636-x

Hosseinzadeh, S., Vanierschot, M., Norman, F., Verplaetsen, F., Berghmans, J., 2018. Flame propagation and flow field measurements in a Hartmann dust explosion tube. Powder Technol. 323, 346–356. doi:10.1016/j.powtec.2017.10.001

Julien, P., Vickery, J., Goroshin, S., Frost, D.L., Bergthorson, J.M., 2015a. Freely-propagating flames in aluminum dust clouds. Combust. Flame 162, 4241–4253. doi:10.1016/j.combustflame.2015.07.046

Julien, P., Vickery, J., Whiteley, S., Wright, A., Goroshin, S., Bergthorson, J.M., Frost, D.L., 2015b. Effect of scale on freely propagating flames in aluminum dust clouds. J. Loss Prev. Process Ind. 36, 230–236. doi:10.1016/j.jlp.2014.12.022

Kahlili, I., 2012. Sensibilité, sévérité et spécificités des explosions de mélanges hybrides gaz/vapeurs/poussières.

Kalejaiye, O., Aymotte, P., Pegg, M., Cashdollar, K., 2010. Effectiveness of dust dispersion in the 20-L Siwek chamber. J. Loss Prev. Process Ind. doi:10.1016/j.jlp.2009.05.008

Li, G., Yang, H.X., Yuan, C.M., Eckhoff, R.K., 2016. A catastrophic aluminium-alloy dust explosion in China. J. Loss Prev. Process Ind. 39, 121–130. doi:10.1016/j.jlp.2015.11.013

Mercer, D.B., Amyotte, P.R., Dupuis, D.J., Pegg, M.J., Heij, W.B.C. De, Zevenbergen, J.F., Scarlett, B., 2001. The influence of injector design on the decay of pre-ignition turbulence in a spherical explosion chamber. J. Loss Prev. Process Ind. 14, 269–282.

Murillo, C., 2017. Experimental and numerical approaches to particles dispersion in a turbulent flow : application to dust explosions.

Proust, C., 2006. A few fundamental aspects about ignition and flame propagation in dust clouds. J. Loss Prev. Process Ind. 19, 104–120. doi:10.1016/j.jlp.2005.06.035

Pu, Y. kang, 1988. Fundamental Characteristics of Laminar and Turbulent Flames in Cornstarch Dust-Air Mixtures.

Sabard, J., 2013. Étude de l 'explosion de mélanges diphasiques : hydrogène et poussières.

Skjold, T., 2003. Selected aspects of turbulence and combustion in 20-Litre explosion vessels: Development of Experimental Apparatus and Experimental Investigation.

Tamanini, F., 1990. Turbulence effects on dust explosion venting. Plant/operations Prog. 9, 52–60. doi:10.1002/prsb.720090111

Vissotski, A., Camou, A., Mannan, S., Petersen, E., 2012. Development of an Experimental Facility for Flame Speed Measurements in Powdered Aerosols. Spring Tech. Meet. Cent. States Sect. Combust. Inst. 2–8.

Wang, S., Pu, Y., Jia, F., Gutkowski, A., Jaronsinski, J., 2006. An Experimental Study on Flame Propagation in Cornstarch Dust Clouds. Combust. Sci. Technol. 178, 1957–1975. doi:10.1080/00102200600790979

Xu, H., Wang, X., Li, Y., Zhu, P., Cong, H., Qin, W., 2017. Experimental investigation of methane/coal dust explosion under influence of obstacles and ultrafine water mist. J. Loss Prev. Process Ind. 49, 929–937. doi:10.1016/j.jlp.2017.04.016

Zhang, X., Yu, J., Sun, J., Gao, W., 2016. Effects of turbulent intensity on nano-PMMA flame propagation behaviors. J. Loss Prev. Process Ind. 44, 119–124. doi:10.1016/j.jlp.2016.09.001